Solving the Inverse Scattering Problem: the Linear Sampling Method

Ana Jocelijn Cavero Roeper
5536995
Utrecht University

A thesis submitted for the degree of
Bachelor of Science
30th June 2017

Major: Physics and Mathematics
Thesis supervisor: dr. Tristan van Leeuwen
Second reader: dr. Viktor Blasjo

Abstract

Scattering occurs when a wave is forced to deviate from its original trajectory by a material object in its path; reconstructing this object, or scatterer, from measurements of the outgoing scatterred wave, is referred to as the inverse scattering problem. Mathematically, this problem is modelled by the Helmholtz equation, the time-independent component of the scalar wave function, and, for a penetrable scatterer, classical methods such as the Born approximation and constrained optimization techniques are discussed in this paper, to motivate the requirement of a new method. Although the classical methods are highly efficient, they require a significant amount of a priori data, which is not always available; the Linear Sampling Method (LSM), however, was introduced by Andreas Krisch and David Colton as a rapid method that requires only a limited number of assumptions. The LSM is discussed in detail and even applied to existing data via a python programme. To conclude, the classical Helmholtz equation is compared to the quantum physical Schrödinger equation; although these equations seem to be rather similar, no analogy between the two could be drawn to apply the LSM to the latter. Regardless, the author notes that the similarities should not be ignored and suggests that it may be possible to modify the LSM to apply to the Schrödinger equation.

Contents

1 Introduction

Scattering occurs when a wave, or beam of particles, interacts with a material object in its path: the wave is forced to deviate from its original trajectory, which generally results in a wave propagating radially outwards. Figure 1 below depicts an incident plane wave of velocity v1 interacting with a scatterer, which causes an outgoing radial wave of speed v2. As can be expected, the resulting scattered wave depends on the physical make-up of the scatterer; in other words, the scattered wave carries information about the unknown material object, which can then be measured. Reconstructing the scatterer from these measurements is referred to as the inverse scattering problem. In this paper, I investigate how to solve the

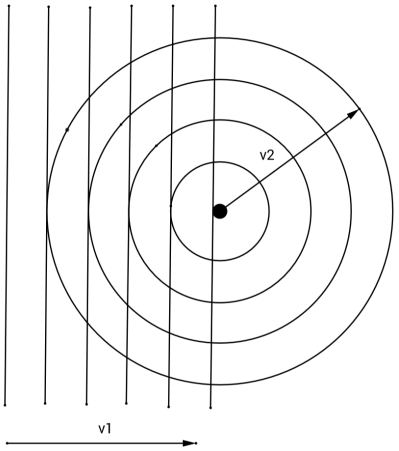

Figure 1: Incident plane wave interacting with unknown scatterer resulting in a radial outgoing wave.

mathematical formulation of the inverse scattering problem with a particular focus on the Linear Sampling Method (LSM) first presented in 1996 by Andreas Kirsch and David Colton. In section 2, I introduce the relevant background information required to understand this topic, outlining the Schrödinger and Helmholtz equations and formulating the inverse problem for two possible cases of scatterers for the latter. From there, I go on to discuss the so-called 'classical techniques' applied to the Helmholtz equation in section 3, to motivate the requirement of the LSM, which I will present in section 4, following F. Cakoni et. al. in "The Linear Sampling Method in Inverse Electromagnetic Scattering". In section 5 I shall outline a project of my own, which consists of a python programme I created to apply my research to existing data published in "Special section: Testing inversion algorithms against experimental data" by Kamal Belkebir and Marc Saillard. Finally, I shall conclude by drawing a similarity between the Schrödinger and Helmholtz equations and investigate the applicability of LSM on the former in section 6. Nevertheless, I shall begin by outlining the general nature of the inverse scattering problem and its applications in modern day science first.

1.1 The Inverse Scattering Problem

Consider a scatterer made up of finitely many parallel cylinders, infinite in length and embedded in a background medium, whose shape and location are to be determined. We assume that this scatterer can be probed using a known incident field emitted by line sources. (Juxtaposed against a point source, in a line source, the electromagnetic radiation emanates from a 1D linear geometry.) The resulting plane wave then propagates through the background medium and interacts with the scatterer.[1] (See figure 1 for a schematic diagram.) The first important part is modelling the incident and scattered waves using a wave function. Since the incident wave is unperturbed, this is (relatively) simple: physics allows us to describe these waves using a second order differential equation; which one to use depends on the nature of the problem, i.e. whether we are talking about a light beam, sound waves or water changes the equation

applied. In the case of the scattering of light, otherwise known as electromagnetic radiation, classically, the wave satisfies the Helmholtz equation, which is introduced in more depth in section 2.2. For the scattered wave, however, it becomes slightly more complicated. Near the source of disturbance, i.e. the scatterer, the wave is rather chaotic and difficult to model.Thus, we must observe the so-called 'far field', where the scattered wave resumes a more ordered state and - once again - can be modelled using a wave equation. (The near and far fields are explained in more depth in appendix A.)
Although in theory we assume full knowledge of the scattered fields, in practice, only limited measurements can be done of the total wave (incident and scattered wave). It is physically impossible to have the required infinite measurements since there are only finitely many transmitting and receiving antennas. Nevertheless, from these measurements we still wish to extract information about the scatterer, such as it's location and shape. This turns out to be more difficult than initially anticipated. Besides being non-linear, the inverse problem is ill-posed following the definition published by Jacques Hadamard in 1902. In order for a problem to be well-posed, Hadamard defined 3 conditions that have to be met, namely: (1) a solution to the problem must exist, (2) the solution has to be unique and (3) the solution's behavior must change continuously with the initial conditions. Thus, a problem is ill-posed if at least one of these conditions is not met. In the case of the inverse scattering problem, conditions (1) and (3) are not always met. In fact, in order to meet Hadamard's second requirement, the Sommerfeld radiation condition has to be applied; as noted later on, this condition is of critical importance to uniquely define the problem.
When a problem, like ours, is ill-posed, it needs to be reformulated for numerical treatment. This process, (called regularization,) is crucial for a reliable solution. A nice way to visualize this process is by comparing it to finding a single solution for the intersection of three lines. There are three possible cases for solving this set of simultaneous equations: The first is a well-posed problem with a single, unique, solution. The other extreme is no solution; the case of three parallel lines that do not intersect. Finally, we arrive at the third, and most relevant, case, which is depicted in figure 2. For this case, there is no unique solution: there

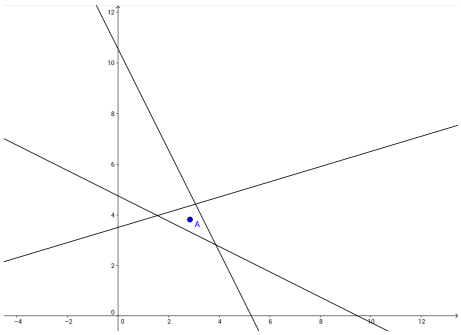

Figure 2: Three lines with no single point where all three lines intersect.

is no single point where all 3 lines intersect simultaneously. However, if necessary, a 'solution' could still be defined and obtained. In that case, the centre of the triangle formed by the three lines (point A in the above figure) could be considered as the solution to the system of equations thereby converting this case into a minimization problem. The methods applied to the inverse scattering problem each try to achieve a similar kind of approximation, each based on (slightly) different assumptions and each with their own bonuses and drawbacks. (Similarly, in the LSM, Tikhonov regularization is applied to obtain a solution, discussed in section 4.1.)
Yet, despite the complexity of the inverse problem in general, it is still a worthwhile problem to study. In fact, although this paper focuses on the mathematical methodology in solving the inverse problem, scattering theory is important across many disciplines.

1.2 The Importance of Scattering Theory

Scattering theory is essential in fields such as nuclear and atomic physics; a lot of our knowledge in these areas comes from scattering experiments such as the Davisson-Germer experiment and the Rutherford gold foil experiment. The Davisson-Germer experiment was conducted by Clinton Davisson and Lester Germer from 1923 to 1927 and was the first measurement of the wavelengths of electrons, an essential discovery for the field of quantum mechanics. The experiment consisted of directing a beam of electrons onto the surface of a piece of nickel and observing how many electrons bounced off at different angles, with the original objective of studying the surface of the piece of nickel. However, in 1925, one of their samples was inadvertently recrystallized in a laboratory accident that changed its structure into nearly monocrystalline form. Their previous polycrystalline samples had exhibited a very smooth angular distribution of scattered electrons, but for this particular sample they found, to their surprise, that at certain angles there was a peak in the detected intensity of the scattered electron beam. As Davisson and Germer later discovered, other monocrystalline samples also exhibited such "anomalous patterns".[2] The peaks in intensity show the wave nature of electrons, and can be interpreted using Bragg's law to give values for the lattice spacing in the nickel crystal. Their later measurements "completely confirmed the quantum mechanical predictions for electron wavelength λ as a function of momentum p: $\lambda = h/p$."[2] Thus, their scattering experiment confirmed the de Broglie hypothesis, advanced by Louis de Broglie in 1924, which states that particles have wave-like properties, and played an important role in the historical development of the Schrodinger equation and quantum mechanics in general.

On the other hand, the Rutherford gold foil experiment, also known as the Geiger-Marsden experiment, had massive implications for classical and nuclear physics as well as chemistry. These series of experiments, conducted by professor Hans Geiger and his pupil Ernest Marsden under the direction of Ernest Rutherford, proved that the mass and positive charge of each atom is concentrated in its centre, namely the nucleus. Prior to the experiment, atoms were described using what popular science has come to call the "plum pudding model"; devised by Lord Kelvin and further developed by J. J. Thomson, this model described the atom as an electrically neutral "assemblage of [negatively charged] corpuscles".[3] The experiments conducted by Geiger and Marsden consisted of bombarding a thin (gold) foil with alpha particles, (discovered by Rutherford in 1899,) which, according to Thomson's model, should have travelled straight through the metal foils. However, Geiger and Marsden observed alpha particles bouncing off the metal foil in all directions: most particles passed through empty space and experienced negligible deviation, but a handful struck the nuclei of the atoms and bounced right back, providing strong evidence against Thomson's model of the atom. Rutherford thus proposed a model of his own: an atom consisting of mostly empty space that has its positive (or negative) charge concentrated in its center. [4] This discovery, based on the results of the alpha particle scattering experiments, was pivotal for science as the newfound atomic structure had implications for a wide range of fields including, physics, chemistry and engineering.

In fact, both these two previously descrived scattering experiments revealed key facts in modern day science, as have many other scattering experiments. Another important scattering process worthy of noting is neutron scattering, an experimental technique used in, among others, crystallography, biophysics, and materials research. In this method, neutrons are directed at a sample: The scattering of neutrons by atoms in the sample allows researchers to determine the relative positions of the atoms and infer information on the atoms' movements, based on the change in direction and velocity of the neutrons. This method, which makes use of neutrons flowing out from a nuclear reactor, was first developed by Betram N. Brockhouse and Clifford G. Shull at the first nuclear reactors in the USA and Canada in the 1940s and l950s, when these "relatively simple and not-too-powerful" nuclear reactors were first made available to researchers after the end of World War II.[5] The contributions by Brockhouse and Shull led to various other significant discoveries like the 1987 Nobel Prize awarded to Bednorz and Müller for "their important break-through in the discovery of superconductivity in ceramic materials" and the 1991 Nobel Prize to de Gennes for "discovering that methods developed for studying order phenomena in simple systems can be generalized to more complex forms of matter, in particular to liquid crystals and polymers."[5] In 1994, Brockhouse

and Shull themselves were jointly awarded the Nobel Prize in physics "for pioneering contributions to the development of neutron scattering techniques for studies of condensed matter". [5]
For a long time, it was most common to study the effects a known scatterer had on an incoming, or incident, wave, rather than the inverse, namely determining the properties of a scatterer based on the scattered wave, probably because the forward problem, as the former is called, is much more straightforward. In fact, translating this physical system into mathematics, we obtain a well-studied forward problem: namely a linear second order partial differential equation whose solution we can determine with certain boundary conditions. The inverse problem, however, namely figuring out what the scatterer is like from (possibly incomplete) information on both the incoming and outgoing waves, is not only more difficult, but also ill-posed in the sense of Hadamard. Nonetheless, the inverse scattering problem is becoming increasingly important, particularly in the field of quantum physics, where scattering potentials cannot be directly measured, thus techniques to infer information from the scatterer are very useful. Several techniques, such as the Born and Kirchhoff approximations, have already been applied in an attempt to resolve the issue and, in some cases, such as with neutron scattering, are sufficiently accurate. Before delving any further into the topic, some basic, yet relevant, concepts required to understand both the classical approaches as well as the more recent Linear Sampling Method are introduced in the subsequent section.

2 Background Information: Modelling the Physical Problem

2.1 The Schrödinger Wave Equation

A wave equation is a linear second order partial differential equation that describes waves in time and space, whether that be waves on a string, in water, or the wave nature of particles. One such wave equation is the Schrödinger equation, which governs quantum mechanical behaviour, describing the time evolution of the wavefunction Φ of a particular system. In other words, the Schrödinger equation describes particles as waves propagating through space-time.[6] The time-indepenedent version of this, in quantum physics well-known equation, is given by

$$-\frac{\hbar^2}{2m}\frac{\partial^2}{\partial x^2}\Phi + V\Phi = E\Phi\,. \tag{1}$$

Equation (1) comes from the eigenvalue problem $H\Phi = E\Phi$ where E is the eigenvalue – in mathematics more generally labelled as λ – corresponding to the energy associated with the state Φ in a particular mode. Thus, ino ther words, the Hamiltonian describes the dynamics of the quantum system, corresponding to the total energy, namely the sum of the potential and kinetic energy, and is of the form: $H = -\Delta + V$.[6] The derivation of the time-independent Schrödinger equation from the eigenvalue form can be found in appendix B.
Generally, the focus lies on determining values of the parameter λ, which can be obtained from a given set of functions that represent the intrinsic or material properties of a system. In other words, it is most common to try to calculate the energy eigenvalues E from the known potential V. Nevertheless, the converse problem, namely reconstructing the scattering potential V from a set of energy eigenvalues E_n, is also of interest, particularly because, in experiments, the scattering potential of a system cannot be obtained directly, but rather the energy states of the scattered wave are measured.[7] This inverse problem is more generally referred to as inverse potential scattering since we are trying to figure out the unknown potential that has scattered the incident beam. Regardless, as can be anticipated, this inverse problem is more problematic in solving than the direct problem; hence, I shall begin by looking at a similar, but slightly simpler, wave equation, namely the Helmholtz equation, first.

2.2 Formulating the Inverse Problem for the Helmholtz Equation

The Helmholtz equation is yet another linear second order partial differential equation; this wave equation is time-independent and arises from the following classical (scalar) wave equation:

$$\frac{\partial^2}{\partial t^2} u = c^2 \Delta u \,, \tag{2}$$

when the wave $u(r,t)$ is assumed to be separable, namely, $u(x,t) = u(x)T(t)$. By substituting this into equation (2) we obtain that

$$\Delta u(x) = k^2 u(x).$$

This technique is referred to as separation of variables.[1] Due to its relationship with the scalar wave equation, the Helmholtz equation often arises when discussing physical problems in space and time, particularly in areas of physics like electromagnetic radiation, seismology and acoustics. In this case, we mainly focus on its application to electromagnetic radiation and the inverse problem of finding the location and shape of the scatterer from data on the scattered wave.

Once again, consider the situation of an unknown scatterer made up of finitely many cylinders and an incoming electric field. Under the assumption that the electric field E is polarized in the x_3 axis, $E(x,t)$ is given by

$$E(x,t) = (0,0,\mathscr{E}(x_1,x_2,t))^T,$$

where $x = (x_1,x_2,x_3)$. James Clerk Maxwell derived (an early form of) the equations that describe electromagnetic fields, core equations that govern modern electrodynamics, and was the first to propose that light is an electromagnetic phenomenon and thus a wave. (Maxwell's equations were confirmed through experiments with radio waves in 1887 by Heinrich Hertz and now form the basis of electromagnetism, optics, and circuits.) Maxwell's fundamental equations imply that $\mathscr{E}$ satisfies the scalar wave equation given by equation (2) and since the wave is monochromatic, $\mathscr{E}$ is given by

$$\mathscr{E}(x_1,x_2,t) = \mathrm{Re}\left(u(x_1,x_2,)e^{-i\omega t}\right) \,, \tag{3}$$

where u is the independent of time and ω is the angular frequency, namely the angular displacement per unit time, related to regular frequency f by $\omega = 2\pi f$. (The units of angular frequency are radians per second.) The brief derivation of the expression for E and the monochromatic wave $\mathscr{E}$ can be found in appendix D.

Recall the derivation of the Helmholtz equation from the scalar wave equation (2) by separation of variables; note that $\mathscr{E}$ is separable, which means that the spacial component $u(x_1,x_2)$ satisfies the Helmholtz equation. The so-called wavenumber k is defined as $k \equiv {}^{\omega}/_{c_0}$, where c_0 is assumed to be constant for both in-, as well as outside, of the scatterer. (This is not necessarily the case; depending on the medium the value of c may be different inside the scatterer from its value outside of the scatterer, but, for now, we shall assume that this is not the case.) The total field u is measured, where

$$u = u^i + u^s \,. \tag{4}$$

The probing or incident field, denoted by u^i, is the field emitted by the line sources that would propagate if there were no scatterer present. This is assumed to be a smooth solution of the background (Helmholtz) equation far from the source. Thus,

$$\Delta u + k^2 u = 0 \,, \tag{5}$$

since nothing has interfered with the wave (yet). Under the assumption that the speed of light c is constant and that the scatterers are far from the antenna we can assume that near the scatterers the incident field is a plane wave given by

$$u^i = e^{ikx\cdot d} \,,$$

[1] For the full working and the solution to the direct problem using separation of variables see appendix C.

where d is a unit vector $d = (d_1, d_2)$ representing the direction of propagation of the wave with wavelength λ, where

$$\lambda = \frac{2\pi}{k} = \frac{2\pi c}{\omega} = \frac{c}{f}\,.$$

The scattered field is produced by the interaction of the incident field with the scatterers. The scattered field originates at the scatterer and propagates (radially) outwards. This physical consideration then motivates the requirement of the scattered field to satisfy the Sommerfeld radiation condition

$$\lim_{r\to\infty} r^{1/2}\left(\frac{\partial u^s}{\partial r} - iku^s\right) = 0\,, \tag{6}$$

where $r = \sqrt{x_1^2 + x_2^2 + x_3^2}$ in 3 dimensions.[8] The Sommerfeld radiation condition ensures the uniqueness of the solution. If the speed of light c is not assumed to be constant, then more complex radiation condition may be necessary instead. (For more on the Sommerfeld radiation condition see appendix E.) Although the equations (4), (5) and (6) do not uniquely determine u^s, since it is not specified how the incident field interacts with the scatterer, such knowledge should not be needed to solve the inverse scattering problem of determining the shape. Nevertheless, the details of the scattering mechanism will determine how well we can find the shape of the scatterer; if the scatterer is almost transparent we will have more difficulty in determining its shape compared to a strongly reflecting object.[1]
As mentioned previously, it is assumed that the scattered field is measured far from the scatterer. It can be shown that the scattered field has the asymptotic expansion far from the scatterer given by:

$$u^s(x) = \frac{e^{ikr}}{\sqrt{r}}u_\infty(\hat{x}, d) + O\left(\frac{1}{r}\right)$$

as $r \to \infty$.[1] The function u_∞ is called the far field pattern of the scattered field. It depends on the incident direction d and the measurement direction $\hat{x}$, as well as the wavenumber k and on the scatterers. It is assumed that u_∞ is known completely; however, in reality, there are only finitely many receiving and transmitting antennas, which means that our knowledge of u_∞ is incomplete. Regardless, although exact knowledge of u_∞ does indeed uniquely determine the boundary of the scatterers in a wide variety of cases, the inverse problem is both nonlinear and ill-posed because this does not imply "the continuous dependence of the reconstruction on the far field data."[1] Nevertheless, there are several classical inversion methods that have already been applied to this problem, discussed in section 3. These techniques apply only to one of two cases: the penetrable scatterer and the extreme case of a perfectly reflecting scatterer. (There is no such thing as a transparent scatterer, as transparent by definition would mean that light passes through the object without being scattered.)

2.2.1 The Perfectly Reflecting Scatterer

Consider first scatterers at high frequencies. If the scatterer is perfectly reflecting, the field is unable to enter the scatterer and Dirichlet boundary conditions apply. Named after Peter Gustav Lejeune Dirichlet, these boundary condition specifies the values that a solution needs to take on along the boundary of the domain when imposed on an ordinary or a partial differential equation. Thus, we obtain the following set of equations, where D is the bounded scatterer with boundary ∂D, $\mathbb{R}^2 \setminus D$ represents the real numbers outside the scatterer and $\bar{D}$ includes the boundary:

$$\begin{aligned} \Delta u + k^2 n(x) u &= 0 && \text{in } \mathbb{R}^2 \setminus \bar{D}\,, \\ u &= u^i + u^s && \text{in } \mathbb{R}^2 \setminus D\,, \\ u &= 0 && \text{on } \partial D\,, \end{aligned}$$

$$r^{1/2}\left(\frac{\partial u^s}{\partial r} - iku^s\right) \to 0 \qquad \text{as } r \to \infty\,.$$

Applying the boundary conditions, we obtain the following far field pattern:

$$u_\infty(\hat{x}, d) = \frac{-e^{i\pi/4}}{\sqrt{8\pi k}} \int_{\partial D} \frac{\partial u}{\partial v}(y) e^{-ik\hat{x}\cdot y} ds(y)\,.$$

It can be noted that this is a nonlinear equation for ∂D in terms of u_∞. In order to solve this problem, intricate techniques are necessary that take into account the boundary conditions. Although in this paper the methods used to solve this particular problem are not discussed, one of these methods, called the Kirchoff approximation, is outlined in appendix F. The slightly simpler case of a penetrable scatterer, on the other hand, will be discussed in more depth.

2.2.2 The Penetrable Scatterer

Now consider the case of a penetrable scatterer with an internal speed of light $c(x_1, x_2) \neq c_0$. If we define $n(x)$ as $n(x) \equiv c_0^2/c^2$ we note that $n(x) = 1$ outside the scatterer and $n(x) \neq 1$ otherwise. This implies a complete set of equations for solving the forward problem, that is, if it is assumed that $n(x)$ is known, namely finding u and u^s such that:

$$\begin{aligned} \Delta u + k^2 n(x) u &= 0 && \text{in } \mathbb{R}^2\,, \\ u &= u^i + u^s && \text{in } \mathbb{R}^2\,, \\ r^{1/2}\left(\frac{\partial u^s}{\partial r} - iku^s\right) &\to 0 && \text{as } r \to \infty\,. \end{aligned} \tag{7}$$

For a wide class of functions $n(x)$, the forward problem is well-posed.[1] The far field pattern is given by

$$u_\infty(\hat{x}, d) = -e^{i\pi/4}\sqrt{\frac{k^3}{8\pi}} \int_{\mathbb{R}^2} e^{-ik\hat{x}\cdot y} m(y) u(y) ds(y)\,, \tag{8}$$

where $m = 1 - n$. In the case of the inverse problem, it is assumed that u_∞ is known and m is unknown; hence, equation (8) provides a nonlinear equation for m.

3 The Classical Methods

3.1 Born Approximation

The Born approximation is an approach based on weak scattering, first proposed by Born in 1926. Weak scattering, also referred to as single scattering, is when radiation is only scattered by a single localized scattering center. The Born approximation approach is still in use, namely for neutron scattering.
This very effective first approach assumes the scattered field to be small juxtaposed against the incident field. Thus, from (7), we see that $u \simeq u^i$. Plugging in u^i for $u(y)$ in the far field pattern given in equation (8) we obtain

$$u_\infty(\hat{x}, d) \simeq -e^{i\pi/4}\sqrt{\frac{k^3}{6\pi}} \int_{\mathbb{R}^2} e^{-ik(\hat{x}-d)\cdot y} m(y) ds(y)\,,$$

where u^i is a plane wave in the direction d. If $\hat{x}$ and d are varied over all possible angles Ω, note that the Born approximation to the far field pattern $u_\infty(\hat{x}, d)$ gives an approximation to the Fourier transform of m for various values of the transform parameter $\epsilon = k(\hat{x} - d)$. Since $|\epsilon| \leq 2k$, the entire Fourier transform is not available; in fact, it leaves us with the problem of computing a band-limited inverse Fourier transform of u_∞ (to determine m) that is ill-posed.[2]

[2]Since we have incomplete or band-limited data.

The Born approximization is popular because it is "computationally efficient and often very successful".[1] For instance, in neutron scattering, the first-order Born approximation is almost always appropriate, with a few exceptions. Regardless, the method is based on weak scattering, i.e. linearizing about the incident field, which may not always be applicable, like with multiple scattering or strong scattering. Also, if m is too large then the approximation will also not be accurate.
As the name suggests, multiple scattering occurs when there are multiple scatters that interfere with the incident wave rather than one. In order to adjust for multiple scattering, the distorted Born approximation was devised and has been used multiple times since, among others in condensed-matter research, namely to analyze grazing-incidence small-angle scattering, a technique used to study nanostructured surfaces and thin films.[9] However, the most common alternative uses constrained optimization techniques, discussed in the following section. (For further reading on the distorted born approximation, the article 'Calculation of Scattering by the Distorted Wave Born Approximation' by Kathie E. Newman and Eytan Domany provides a nice overview, see [9].)

3.2 Constrained Optimization Techniques

In the case of strong, or multiple, scattering, the prevalent alternative is to explicitly indicate that u depends on the unknown function m. This is done by denoting the total field at x once again for the case of the penetrable scatterer, for any suitable $\tilde{m}$, by $u(x, \tilde{m})$, where $n = 1 - \tilde{m}$. The far field pattern obtained from (8) in this case is given by:

$$u_\infty(\hat{x}, d, \tilde{m}) = -e^{i\pi/4}\sqrt{\frac{k^3}{8\pi}}\int_{\mathbb{R}^2} e^{-ik\hat{x}\cdot y}\tilde{m}(y)u(y, \tilde{m})ds(y).$$

In other words, the problem is converted into a minimization problem following a similar idea as the intersecting lines presented previously in section 1.1. Taking $u_\infty^{\text{meas}}(\hat{x}, d)$ to be the measured data of the far field pattern, a "suitable admissible set A of possible functions $\tilde{m}$" is chosen.[1] Using so-called constrained optimization techniques, an optimal best fit to the data is computed by solving:

$$m^* = \arg\min_{\tilde{m}\in A} \int_\Omega \int_\Omega |u_\infty^{\text{meas}}(\hat{x}, d) - u_\infty(\hat{x}, d, \tilde{m})|^2 ds(d)ds(\hat{x})\,. \tag{9}$$

Constrained optimization techniques are generally iterative procedures such as the integral equation techniques referred to by Cakoni et. al.; the forward problem for different $\hat{m}$ is solved multiple times, which means that this process is fairly slow. By generalizing equation (9), these techniques "can handle a wide variety of data and constraints."[1] However, these techniques are still expensive and prone to errors, since the possibility of stopping at a local minima[3] is high.

4 The Linear Sampling Method

As discussed in the previous section, several very efficient linearized techniques can be constructed based off of band-limited Fourier transforms. However, although efficient, these methods require very strong a priori data. In "The Linear Sampling Method in Inverse Electromagnetic Scattering", Cakoni et. al. describe the linear sampling method (LSM) as an alternative that requires very limited a priori data. The LSM is pretty fast compared to the optimization methods presented earlier and only involves the solution of linear ill-posed problems. Regardless, this technique is not perfect. LSM needs substantially more input data than both optimization approaches and asymptotic methods.

[3] the smallest value within a given range, not necessarily of the entire domain of the function

The LSM was first presented in a paper by Andreas Kirsch and David Colton in 1996. The LSM is based on the so called 'far field equation', namely finding a function $g_z \in L^2(\Omega)$ such that

$$\int_\Omega u_\infty(\hat{x}, d) g_z(d) ds(d) = \Phi_\infty(\hat{x}, z)\,, \tag{10}$$

where Φ_∞ is the far field pattern due to a point source located at the auxiliary point z. In 2 dimensions, this field is given in the near field by the following expression[1]:

$$\Phi_\infty(x, z) = \frac{i}{4} H_0^{(1)}(k|x - y|)\,. \tag{11}$$

$H_0^{(1)}$ is the Hankel function of first kind of order zero. The far field pattern is given by

$$\Phi_\infty(\hat{x}, z) = \frac{e^{r^\pi/_4}}{\sqrt{8\pi k}} e^{-ik\hat{x}\cdot z}\,. \tag{12}$$

Next $\psi(z) = ||g||^{-1}_{L^2(\Omega)}$ is taken as an indicator function for the scatter D as z varies over $\mathbb{R}^2$. $\psi(z)$ is approximately zero outside D.
Generally, equation (10) is ill-posed in the sense of Hadamard; u_∞ is an analystic function of $\hat{x}$ and d. The ill-posedness "calls into question the existence of solutions" to equation (10).[1] Hence, in order to approximate the solutions numerically, regularization techniques have to be used. Regardless, assuming that there exists a solution for some $z \in \mathbb{R}^2$, using Rellich's Uniqueness Lemma (given in appendix H) and the fact that both sides of equation (10) are far field patterns the expression

$$\int_\Omega u^s(x, d) g_z(d) ds(d) = \Phi(x, z) \qquad\qquad x \in \mathbb{R}^2 \setminus D \tag{13}$$

is obtained. It follows that equation (10) does not have a solution for each $z \in \mathbb{R}^2$. (To show this take $z \in \mathbb{R}^2 \setminus \bar{D}$ and note that equation (13) above cannot hold since the left hand side of equation (13) is bounded in L^2 on compact subsets of $\mathbb{R}^2 \setminus D$, yet the norm of Φ is unbounded if the subset contains z.[1]) Assume, however, that equation (10) has a solution for each $z \in D$. Applying Dirichlet boundary conditions, x is fixed such that $x \in \partial D$ and z is allowed to approach x from inside the scatterer D. Note that the $L^2(D)$ of the right hand side of equation (13) blows up, which implies that the norm of the left hand side should also do so. Since the scattered field u^s is bounded, $||g_z||_{L^2(\Omega)} \to \infty$ as $z \to x$. By using the regularization method presented in the following section (4.1), the indicator function $\psi(z)$ given previously should approach 0 as z approaches ∂D from the inside and be roughly zero for $z \ni D$. In other words, g_z should be a nice way to (qualitatively) visualize D.[1] However, in general, equation (10) only has an exact solution for very few domains; LSM is thus based on the fact that there is an *approximate* solution with the desired 'blowup' as z approaches ∂D.
In summary, the LSM consists of 3 main steps. First, using a priori data on the approximate size and location of the scatterer, the parameter z is varied over a grid in the region where the scatterer D is sought. For this to work, the grid has to be "fine enough" and D needs to be within the search domain. Step 2 consists of using each z to approximately solve equation (10) and compute g_z. To do this we use regularization techniques, which will be discussed in the next section. Lastly, the indicator function $\psi(z) = ||g||^{-1}_{L^2(\Omega)}$ is plotted and information about the scatterer can be extracted using for instance a contour value C and the level curve $\psi(z) = C$. For this final step, several different methods have been applied including "calibrating" or the "deformable model" approach. The former approach compares the data to computations of forward data of known objects of similar size to the scatterer, whereas the latter adjusts the contour on $\psi(z)$ itself. In "The Linear Sampling Method in Inverse Electromagnetic Scattering", Cakoni et al. use the calibrating method; however, there is no strict guideline (yet) as to which method is better. Regardless, mathematically speaking, the most interesting part of the method is the second step, the regularization techniques, since this is where the 'real work' happens and the inverse problem gets 'solved'.

4.1 Regularization Techniques

Since u_∞ is analytic, regularization techniques need to be applied in order for our indicator to be reliable. In the original proposal of LSM by Kirsch and Colton in 1996, regularization techniques were not used. Since then, these techniques account for some of the improvements of the method.
First N equally spaced directions d around the unit circle are calculated, where the choice of N depends on the wavenumber and the size of the scattering object. d is obtained by taking

$$d_j = (\cos\theta_j, \sin\theta_j), \qquad \theta_j = \frac{2\pi j}{N}, \qquad j = 1, ..., N\,. \tag{14}$$

For instance, if we take $N = 3$ evenly spaced directions around the unit circle we'd obtain:

$$\theta_j = \frac{2\pi j}{3} = \begin{cases} \frac{2}{3}\pi & j = 1 \\ \frac{4}{3}\pi & j = 2 \\ 2\pi & j = 3 \end{cases}.$$

Thus d obtains the following values shown in the unit circle in figure 4.1. According to Cakoni et. al., it is

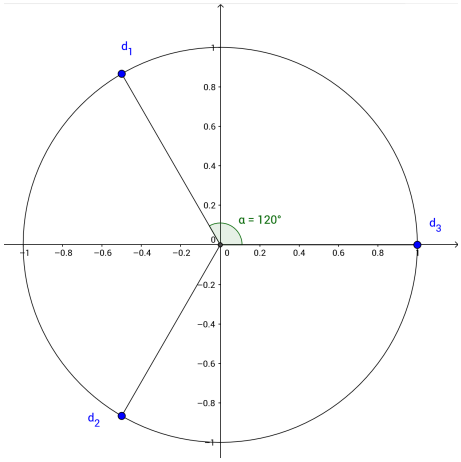

Figure 3: $N = 3$ evenly spaced directions d on the unit circle.

recommended to choose N such that at least $N > 2ka$ where a is the radius of the circumscribing circle for D and k is the wavenumber.
Next, suppose that u_∞ can be approximated by a discrete data matrix u_∞^δ. Using the values of d an $N \times N$ matrix A^δ is defined, where

$$A^\delta_{l,m} = u^\delta_\infty(d_l, d_m).$$

The method assumes that

$$||A - A^\delta|| \leq \delta\,. \tag{15}$$

With numerical data, the first step is to choose a test scatterer and compute a synthetic approximation $u_\infty^{\text{comp}}(d_l, d_m)$ of $u_\infty(d_l, d_m)$ using a finite element method. This is because the problem cannot be solved analytically: instead, an approximation is computed by discretizing the problem in terms of basis functions. Furthermore, in order to avoid so-called "inverse crimes", the synthetic approximation has to be perturbed as follows:

$$u^\delta_{l,m}(d_l, d_m) = u^{\text{comp}}_\infty(d_l, d_m)(1 + \epsilon\xi_{l,m})\,, \tag{16}$$

where ϵ is a positive non-zero parameter, and ξ is a random number from a uniform distribution $-1 > \xi_{l,m} > 1$. (More on inverse crimes can be found in appendix G.) Using the trapezoidal rule, the integral of

equation (10), namely

$$\int_{\Omega} u_\infty(\hat{x}, d) g_z(d) ds(d) = \Phi_\infty(\hat{x}, z)\,,$$

can be approximated, resulting in the following expression:

$$A^\delta \overrightarrow{g_z} = b_z\,, \tag{17}$$

where $b_z \in \mathbb{C}^N$ is given by $(b_z)_l = h^{-1}\Phi_\infty(d_l, z)$ where $1 \leq l \leq N$ and $h = \frac{2\pi}{N}$, for which we seek to compute the indicator function $\overrightarrow{g_z} \in \mathbb{C}^N$. Cakoni et. al. note that in practice, the above expression is highly ill-conditioned as N increases, which can be expected as equation (10), which is being approximated, is ill-posed. To solve the approximation (17), the method applied is Tikhonov regularization.
Tikhonov regularization, explained in some depth in appendix I, requires the solution of

$$\left(\alpha_z I + \left(A^\delta\right)^* A^\delta\right) \overrightarrow{g}_z^\alpha = \left(A^\delta\right)^* \overrightarrow{b_z}\,, \tag{18}$$

where $\left(A^\delta\right)^*$ is the conjugate transpose of A^δ and $\alpha_z > 0$ is the regularization parameter, which Cakoni et. al. pick according to the Morozov Principle. The Morozov Discrepancy Principle is discussed in detail in appendix I.1, but basically revolves around finding α_z such that

$$||A^\delta \overrightarrow{g}_z^\alpha - b_z||^2 = \delta^2 ||\overrightarrow{g}_z^\alpha||^2\,. \tag{19}$$

As we've seen above, this particular method computes a distinct regularization parameter for each z. However, a more recent method that uses only a single parameter has been proposed by Aramini et al. Although this method, referred to as No Sampling Linear Sampling (NSLS), is attractive because "it avoids recomputing the regularization parameter for each z," Cakoni et. al. argue that the performance of the classical regularization technique is good enough.[1] (For more on the linear sampling method with a single regularization parameter, see [10].)

5 Personal Project

To explore the possibilities of the LSM, I decided to apply the LSM to actual data, by constructing a programme in Python that would attempt to solve the Tikhonov regularization equation (18), presented in section 4.1, for actual data. As I do not have the means to collect data of my own, I have used the data presented in "Special section: Testing inversion algorithms against experimental data". Belkebir and Saillard present the results of their scattering experiments with the purpose of sharing these with theoretical scientists that do not have access to usable data, as they are "aware of the importance of testing inversion numerical algorithms against experimental data."[11] To collect their data, Belkebir and Saillard used a so-called '2D bistatic measurement system', depicted in figure 4, in which the scatterer (referred to as the target) is stationed in the centre of the setup. The emitter is fixed whereas the scatterer can rotate. The receiver can move in a ring around the target.
The data is presented in text files, which can be easily accessed in python using the `open()` function. Figure 5 depicts the first 30 lines of the data on the metallic cylinder where the 7 columns correspond to:

1. the emission angle: range $0 - 36$ (corresponding to $0°$ to $360°$ in steps of $10°$)
2. the reception angle: range $13 - 61$ (corresponding to $60° - 300°$ in steps of $5°$)
3. the operating frequency (GHz)
4. the real part of the total electric field
5. the imaginary part of the total electric field

6. the real part of the incident electric field
7. the imaginary part of the total electric field

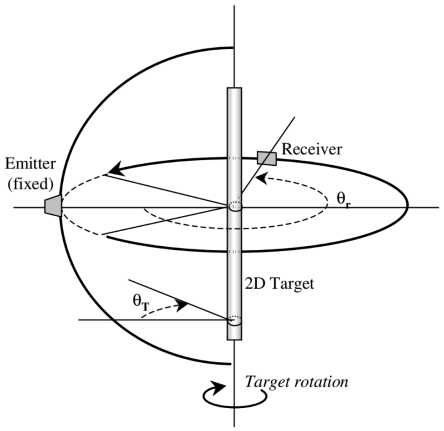

Figure 4: 2D bistatic measurement system with rotating target and receiver, from [11].

The incident and total wave fields for five different configurations of scatterers were recorded at different angles of rotation, as well as using different frequencies of electromagnetic radiation. For more information about the experimental setup and data collected, I refer the reader to [11].

```
# Institut Fresnel, TEM.
# Date : 16/9/1999.
# Object : metallic cylinder.
# Polarization : TM (E //)
# Number of frequencies : 4 (4, 8, 12, 16 GHz)
# Number of views : 36
# Number of receivers : 49 per view.
#
# Contact : K. BELKEBIR, phone: 04 91 28 84 03, email: kamal.belkebir@fresnel.fr
#
  1   13    4    -1.5730E-001     3.9900E-002    -1.7100E-002    -1.2100E-002
  1   13    8    -3.2300E-002    -2.4900E-002     2.8000E-003     4.3000E-003
  1   13   12     2.8300E-002    -1.3500E-003     6.3000E-003     2.5000E-003
  1   13   16    -1.0900E-002     2.5100E-002    -2.0000E-003    -1.8000E-003
  1   14    4    -1.1980E-001     4.3950E-002     1.6500E-002    -1.2200E-002
  1   14    8    -3.8800E-002    -3.0400E-002    -3.8000E-003    -2.1000E-003
  1   14   12     2.4900E-002    -3.9000E-003     3.3000E-003    -3.3000E-003
  1   14   16     1.5000E-003     3.6300E-002     8.0000E-003     6.0000E-003
  1   15    4    -1.3280E-001     7.2000E-002     4.6000E-003     1.7450E-002
  1   15    8    -3.1700E-002    -2.9700E-002     7.0000E-004    -7.0000E-004
  1   15   12     1.8500E-002     3.5500E-003    -4.0000E-003     3.2000E-003
  1   15   16    -6.4000E-003     2.5900E-002    -7.0000E-004    -2.4000E-003
  1   16    4    -1.4680E-001     4.2800E-002    -1.3150E-002    -6.0000E-003
  1   16    8    -3.0300E-002    -2.8700E-002     1.1000E-003     7.0000E-004
  1   16   12     3.0300E-002    -9.0000E-004     8.2000E-003    -9.0000E-004
  1   16   16    -3.5500E-003     3.6000E-002     1.4000E-003     5.6000E-003
  1   17    4    -1.1120E-001     5.5000E-002     1.6900E-002     1.2000E-003
  1   17    8    -2.9100E-002    -2.8500E-002    -2.0000E-004     8.0000E-004
  1   17   12     2.3400E-002    -3.9000E-003     3.0000E-004    -4.4000E-003
  1   17   16     5.2500E-003     3.2400E-002     8.6000E-003     2.5000E-003
```

Figure 5: First 30 lines of textual data file for a metallic cylinder, from [11]

.

First of all, in order to create a programme in Python that could apply the LSM to this data, a couple of things had to be considered, namely (1) the LSM describes different incident and receiving angles, but does not speak of a rotating target, (2) the data doesn't include measurements for the range of angles $0° - 60°$ and $300° - 360°$ and (3) not all combinations of incident and receiving angle are present. The solution to these issues were surprisingly trivial: For the first, the negative angle by which the target is rotated, is equivalent to the positive angle of rotation of the emitter if the target were stationary. The second 'issue' is not a problem: although the LSM specifies that the matrix A^δ to be constructed ought to be an $N \times N$ matrix, it can deal with an $N \times M$ (where $N \neq M$) matrix since it solves equation (18), which makes use of the $N \times N$ matrix $(A^\delta)^* A^\delta$, as presented in section 4.1.[4] As for (3), the missing values are around the $0°$

[4]Nevertheless, it turns out that the Morozov principle cannot be applied to compute the regularization parameter due to this fact, which shall be noted later on.

position, which results in an incomplete, yet still workable, data matrix, as depicted in figure 6.

5.1 The Data Matrix

The first part of the programme constructs a (data) matrix from the text files presented previously. This matrix corresponds to A^δ of the LSM presented in equation (15). In other words, the matrix contains the scattered waves for the different measured positions. Each row corresponds to an angle $-\theta_T$ of the incident wave and each column corresponds to an angle θ_r at which the emitted field was measured, (see figure 4,) i.e. element A_{ij} contains the scattered field measured when the incident angle was $i \times 10$ and the emitter was at angle $j \times 5$. Thus, after filtering the data for a particular (user-requested) frequency, a sorted list of lists had to be constructed, where each list contained one row for the matrix. At this point it was important to assign a value (I chose 0) for the missing measurements. For the construction of the actual matrix in Python, the NumPy package was used, with the main advantage that it can handle multidimensional arrays and, among other functions, compute the conjugate transpose of a matrix and do matrix multiplication. To check whether the matrix made sense I used the MatPlotLib package to plot the real part of the matrix ('data_matrix'):

```
import numpy as np
from matplotlib import pyplot as plt

plt.matshow(np.real(data_matrix))
plt.show()
```

The result for the data file for a metallic cylinder is shown in figure 6. The image makes sense for a metallic cylinder; a certain degree of symmetry is expected and obtained. Similar measurements should be obtained at similar differences in angle between emitter and receiver, which is the case, as can be noted by the similar colors along the diagonal of the matrix in figure 6.

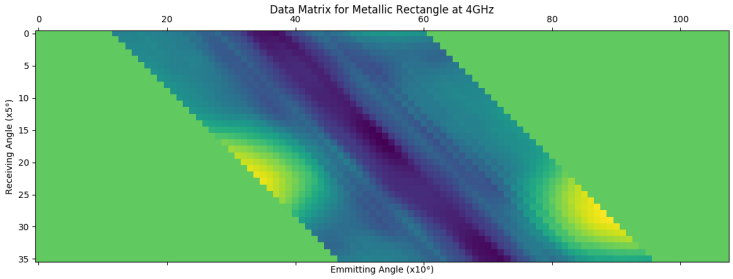

Figure 6: Plot of data matrix for a centred metallic cylinder filtered for frequency 4GHz.

As for computing the transpose of this matrix, the NumPy function `data_matrix.getH()` did the trick.

5.2 Solving the Inverse Problem

As mentioned before, the equation to be solved is given by

$$\left(\alpha_z I + \left(A^\delta\right)^* A^\delta\right) \overrightarrow{g}_z^\alpha = \left(A^\delta\right)^* \overrightarrow{b_z},$$

where the data matrix computed by the programme is A^δ, $(A^\delta)^*$ refers to the conjugate transpose of the data matrix and the vector b_z is given by $(b_z)_l = h^{-1}\Phi_\infty(d_l, z)$. The indicator function g_z is the solution we wish to compute. Having created the data matrix and computed its conjugate transpose, the next step was

to create an array b_z, where each element of the vector corresponded to the incident angle (the rows) of the data matrix. As presented in section 4, the far field pattern Φ_∞ is given by

$$\Phi_\infty(\hat{x}, z) = \frac{e^{r^{\pi}/_4}}{\sqrt{8\pi k}} e^{-ik\hat{x}\cdot z}\,.$$

(As can be noted in the full programme presented in appendix J, code was created to compute g_z in terms of Φ given by equation 11 as well. This was done to compare both results.) Important considerations here regarded the two dimensional vector $\hat{x}$ and coordinate z. First, $\hat{x}$ is a 2 dimensional *unit* vector, i.e. $x = (x_1, x_2)$ is of length unity, that points to the location at which the wave is measured (around the unit circle). z denotes the two dimensional coordinates of a hypothetical point source within a specified domain for which b_z is calculated (and thus g_z is solved) to check whether or not point z lies within the scatterer; if the chosen z does not solve the Tikhonov system of equations, then this point lies inside the scatterer. In terms of the experimental setup, the coordinate x of reception of the wave lies on a circle around the (unknown) scatterer, as shown in figure 7. The scatterer D lies somewhere in the domain G.

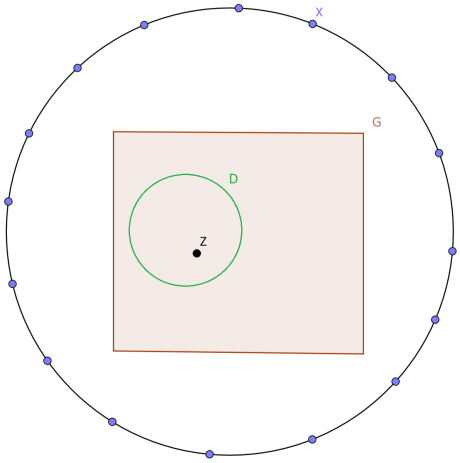

Figure 7: Experimental setup of scatterer D in search domain G, with measurements being made at x.

Thus, to solve the inverse problem, the procedure is as follows: Pick a z on the grid (inside the domain) and check whether or not it solves equation (18). If it does, then this point lies outside the scatterer; if it doesn't then point z is inside the scatterer as depicted in figure 7. This procedure is repeated for all z on the grid in domain G. Obviously, it is important to choose a search domain G smaller than the radius of the experimental setup. In terms of programming, this is a costly procedure; besides the complication of choosing multiple z, running the programme over all these values takes time. Nonetheless, in order to achieve this, I defined a function `computation(z,alpha)` that returns the norm of the indicator function g_z for a given regularization parameter `alpha` and iterated it over a range of z.
To solve the system of equations for a predefined α and z the SciPy package was used; the SciPy package is specialized in all sorts of efficient numerical routines such as integration and optimization, as well as solving a system of equations. For the Tikhonov equation, the indicator function was computed with `g=np.linalg.solve(A,B1)` where `A` was defined as $\left(\alpha_z I + \left(A^\delta\right)^* A^\delta\right)$ and `B1` as $\left(A^\delta\right)^* \overrightarrow{b_z}$, the right- and left-hand side of equation (18) respectively. However, due to the available data from [11], the Tikhonov regularization could not be applied to its fullest extent; since the data matrix was not $N \times N$, the Morozov principle could not be applied as done by Cakoni et. al. to compute the regularization parameter α, as A^δ could not be diagonalized. Thus, the programme uses a user-requested value for the regularization parameter, or otherwise uses a default $= 1 \times 10^{-6}$. (Ideally, α would be recomputed for each individual z.)

Once again, to visualize the result, a matrix of the output was plotted using MatPlotLib; a regularization parameter of 1×10^{-6} was used to obtain figure 8 for two dielectric cylinders filtered for frequency 5GHz. For all the results obtained using the full programme presented in appendix J see appendix K. The result

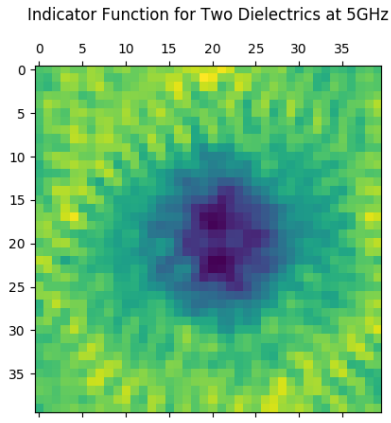

Figure 8: Plot of indicator function for two dielectric cylinders filtered for frequency 5GHz.

obtained in figure 8 is exciting in that it clearly shows a radial wave disturbed by an object (in this case two dielectric cylinders) in the centre. The axes of the plot correspond to coordinates z with z_1 and z_2 in the range $[-0.2, 0.2]$. The two cylinders are not clearly defined in the image, which may be due to the frequency of light used or the regularization parameter α chosen. As can be seen from figures 9(a) and 9(b), the value of α has a significant influence on the output of the programme. Where in figure 9(a) the outermost parts

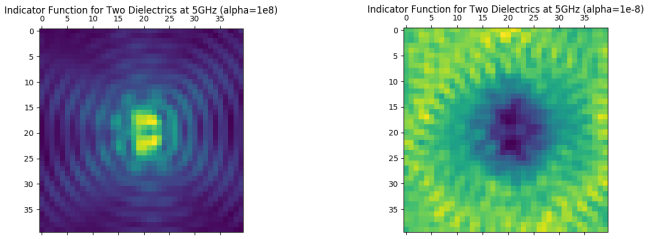

(a) alpha = 1×10^{8} (b) alpha = 1×10^{-8}

Figure 9: Comparison of the indicator function plot of two dielectrics at frequency 5GHz for two different α values.

of the plot denote more clearly the radial wave, the two dielectrics are more easily distinguished in figure 9(b). Moreover, the regularization parameter α used by the programme is the same for each z. This suggests that if α were actually recomputed for each z, where each coloured square corresponds to a coordinate z, the image obtained could be clearer. To emphasize the importance of alpha, appendix K.5 provides several plots of the indicator function for a range of values for α.

6 The Quantum Scattering Problem

Having discussed the classical approaches, as well as Colton and Kirsch's Linear Sampling Method, I return to the Schrödinger equation (1). The existing work on the Schrödinger equation is not that similar to the methods discussed above for the Helmholtz equation. Regardless, the Born approximation has been

applied to solve the inverse potential scattering problem, much in the same way as discussed in section 3.1. Once again, the Sommerfeld radiation condition (6) applies, such that the scattered wavefield Φ^s satisfies

$$\lim_{r\to\infty} r\left(\frac{\partial\Phi^s}{\partial r} - ik\Phi^s\right) = 0\,.$$

Analogous to the far field pattern for the Helmholtz equation presented in section 4 by equation (10), the following expression is obtained for the Schrödinger equation:

$$\Phi(x,t) = \int e^{-ik^2t}\Phi(k,x)f(k)ds(k)\,, \tag{20}$$

where $f(k) \in L^2(\mathbb{R}^{\not\vDash})$ and $\Phi(k,x)$ is the total field, given by

$$\Phi(k,x) = e^{ik\cdot x} - \frac{1}{4\pi}\int \frac{e^{ik|x-y|}}{|x-y|}V(y)\Phi(k,y)ds(y)\,.$$

Like with the total electromagnetic field, this field is composed of both an incident and scattered wavefield, where the incident wavefield is given by the first term ($e^{ik\cdot x}$). Thus, for the Born approximation, it is once again assumed that the scattered field is small juxtaposed against the incident field and the expression for the total field used in (20) becomes

$$\Phi(k,x) = -\frac{1}{4\pi}\int \frac{e^{ik|x-y|}}{|x-y|}V(y)\Phi(k,y)ds(y)\,.$$

The most notable difference is that there is an 'extra' term, namely the potential $V(y)$. Other methods have been used, most involving lengthy integrals, in order to attempt to solve the inverse Schrödinger equation; still, this scattering problem has only been solved for a limited number of cases. The general inverse potential scattering problem is highly complex and, according to Khosrow Chadan in [7], has not yet been completely solved. Regardless, some simpler cases, such as when the potential has spherical symmetry $V(\overrightarrow{x}) = V(|\overrightarrow{x}|)$ have "complete satisfactory solutions".[7]
This latter case can be tackled by decomposing the wave function $\Phi(k,x)$ into partial waves $\phi_l(k,r)$, where $r = |\overrightarrow{x}|$, and using the radial form of the Schrödinger equation,

$$\left[-\frac{d^2}{dr^2} + \frac{l(l+1)}{r^2} + V(r)\right]\phi_l(k,r) = E\phi_l(k,r)\,. \tag{21}$$

As noted by Khosrow Chadan in chapter 4 of "An Introduction to Inverse Scattering and Inverse Spectral Problems", there are two types of inverse potential scattering problems that occur. One is the inverse problem of reconstructing the potential $V(x)$ at fixed energy. The second is solving for the potential at fixed l. (The reader is directed to [7] for more information on these cases and methods.) Note that at $l = 0$ the radial Schrödinger equation simplifies to the time-independent form presented earlier.
As far as I am aware, the LSM has not (yet?) been applied to the Schrödinger equation, due to the 'extra' potential term. Be that as it may, these two equations, the Helmholtz equation (5) and the Schrödinger equation (1), are very similar in form. In order to compare these equations, the dispersion relation has to be introduced first, to rewrite energy in terms of the wavenumber k. A "dispersionless" wave, like those described by the classical wave equation (2), and thus the Helmholtz equation, are waves whose speed doesn't depend on frequency ω or wavenumber k.[12] In the case of the scalar wave equation

$$\frac{\partial^2}{\partial t^2}u = c^2\Delta u\,,$$

the phase velocity of the wave ω/k, namely the velocity of a point with constant phase, $kx - \omega t$, is the constant c, which is independent of ω and k, a result obtained by plugging the solution ($u = Ae^{i(kx-\omega t)}$)

back into the equation to get the dispersion relation $\omega^2 = c^2k^2$. Similarly, for a free particle (zero potential) in quantum physics, we can obtain the following dispersion relation:

$$\omega = \frac{\hbar k^2}{2m}\,,$$

which comes from de Broglie's statement that all particles have wave-like properties, i.e. a frequency ω and wavenumber k can be associated with them, as well as an energy given by $E = \hbar\omega$ and momentum $p = \hbar k$. Using these definitions in the classical formulation of energy, (which for a free particle is given by $E = {}^{p^2}/_{2m}$,) the dispersion relation is found. Thus, assuming the dispersion relation, the time-independent Schrödinger equation takes on the form:

$$-\frac{\hbar^2}{2m}\frac{\partial^2}{\partial x^2}\Phi + V\Phi = \frac{\hbar^2 k^2}{2m}\Phi\,.$$

Next, assuming natural units $c = \hbar = m = 1$ we simplify the equation further. (Natural units are a common understanding in physics; these are units of measurement based only on universal physical constants such as the electric charge e and the speed of light c.) Moreover, redifining V to contain a factor of 2, we can get rid of all constants, such to ease computation:

$$-\frac{\partial^2}{\partial x^2}\Phi + V\Phi = k^2\Phi\,. \tag{22}$$

Equation (22) is a common form of the Schrödinger equation, which is a lot simpler to work with, yet represents the same thing; it is, in fact, very similar to the Helmholtz equation dealt with previously:

$$\begin{aligned}
-\Delta\Phi + V\Phi &= k^2\Phi\,,\\
-\Delta\Phi + V\Phi - k^2\Phi &= 0\,,\\
-\Delta\Phi + (V - k^2)\Phi &= 0\,,\\
\Delta\Phi + (k^2 - V)\Phi &= 0\,,
\end{aligned}$$

where Δ is the Laplace operator. Once again, note the 'extra' potential term. As mentioned previously, the two natural inverse problems are in search of the potential in terms of either constant energy or constant l. However, what if we were to tackle the same inverse problem (of location and shape) as before? It seems as though the k^2 term could be grouped with the potential term into a function of x to obtain the expression

$$\Delta\Phi + K(x)\Phi = 0\,,$$

where $K(x) = k^2 + V(x)$. assuming a priori that the potential is but a constant, $K(x) = K$, we would be dealing with the Helmholtz equation (defining some $\mu = \sqrt{K}$) all over again. However, returning focus to the inverse potential scattering problem, this line of thought does not make much sense; whereas k is a known constant in the inverse Helmholtz problem, the potential $V(x)$ is what we are trying to reconstruct for the inverse problem with the Schrödinger equation. Nevertheless, the similarity between the Helmholtz and the Schrödinger equations cannot be ignored and, thus, provides some food for thought regarding potential methods of solving the latter inverse problem.

7 Concluding Remarks

The inverse scattering problem is an interesting and important topic in modern day physics, as well as other disciplines, because it deals with a wide range of problems. The typical scenario is a sound wave scattering off a metallic ball, or light waves being diffracted by a slit. In the case of the Helmholtz equation discussed in this paper, we consider an electromagnetic (light) wave scattered by an unknown object and wish to

reconstruct the scatterer from measurements of the incident and outgoing waves. Some classical approaches to solving this inverse problem of location and shape of a scatterer exist; the Born approximation and the constrained optimization techniques were discussed in this paper as two of the key methods used. Although these methods are useful in different specific scenarios, the assumptions upon which they are based are a significant limiting factor to their use in terms of applicability and reliability. In fact, although efficient, these methods require very strong a priori data.

The Linear Sampling Method, a method that does not require as much a priori information about the scatterer, is thus a significant and worthwhile improvement. The introduction of the Linear Sampling Method by Andreas Kirsch and David Colton in 1996 provides a way of solving the inverse Helmholtz equation by computing the indicator function g_z without as many assumptions. Nevertheless, the regularization method presented by Cakoni et. al. is a costly process because the regularization parameter α is recomputed for each coordinate z; a more recent approach by Aramini et. al., called "no-sampling linear sampling" is therefore advised. Furthermore, due to the ill-posedness discussed in section 4, a full mathematical justification of the method is lacking; nevertheless, Tilo Arens shows that for a large class of scattering problems linear sampling functions properly in his paper "Why linear sampling works".[13] According to Cakoni et. al. the lack of a mathematical basis "may well be one reason why Andreas Kirsch has developed the more sophisticated "Factorization" method." The Factorization method, not discussed in this paper, has "a stronger mathematical foundation but is more difficult to extend to general scattering problems."[1] Moreover, despite it's wide applicability, the LSM has yet to be applied on different functions, including the mathematically relatively similar (but physically remarkably distinct) Schrödinger equation. This is mainly due to the fact that the inverse potential scattering problem deals with the reconstruction of the potential (as the name suggests) rather than the location of the scatterer. Regardless, comparing both equations it seems likely that the Linear Sampling Method could be adapted to apply to the latter as well. In other words, there is plenty of room for interesting developments. Regardless, in doing so, it is important to keep in mind that the Schrödinger and Helmholtz equations have very different 'meanings' physically, which have to be considered throghout the mathematical process. As Sommerfeld himself notes in his book on partial differential equations in physics[8]:

> We do not really deal with mathematical physics, but with physical mathematics; not with the mathematical formulation of physical facts, but with the physical motivation of mathematical methods. The oft-mentioned "prestabilized harmony" between what is mathematically interesting and is physically important is met at each step and lends an esthetic-I should like to say metaphysical-attraction to our subject."

8 Bibliography

[1] Fioralba Cakoni, David Colton, and Peter Monk. *The Linear Sampling Method in inverse electromagnetic scattering*. SIAM, 2011.

[2] Friedel Weinert. Davisson-Germer experiment. *Compendium of Quantum Physics*, pages 150–152, 2009.

[3] Giora Hon and Bernard R Goldstein. JJ Thomson's plum-pudding atomic model: The making of a scientific myth. *Annalen der Physik*, 525(8-9):A129–A133, 2013.

[4] Ernest Rutherford. The scattering of a and b particles by matter and the structure of the atom. *Philosophy Magazine*, 21:669–688, 1911.

[5] Nobel Media AB. The structure and dynamics of matter revealed. *Nobelprize.org*, 1994.

[6] Ramamurti Shankar. *Principles of quantum mechanics*. Springer Science & Business Media, 2012.

[7] Khosrow Chadan. Inverse problems in potential scattering. *An introduction to inverse scattering and inverse spectral problems*, 2:131, 1997.

[8] Steven H Schot. Eighty years of Sommerfeld's radiation condition. *Historia mathematica*, 19(4):385–401, 1992.

[9] Kathie E Newman and Eytan Domany. Calculation of scattering by the Distorted Wave Born Approximation. *Proceedings of the ARPA/AFML Review of Progress in Quantitative NDE*, 1979.

[10] Riccardo Aramini, Massimo Brignone, and Michele Piana. The linear sampling method without sampling. *Inverse Problems*, 22(6):2237, 2006.

[11] Kamal Belkebir and Marc Saillard. Special section: Testing inversion algorithms against experimental data. *Inverse problems*, 17(6):1565, 2001.

[12] David Morin. *Introduction to classical mechanics: with problems and solutions*. Cambridge University Press, 2008.

[13] Tilo Arens. Why linear sampling works. *Inverse Problems*, 20(1):163, 2003.

[14] Michael I Mishchenko. Far-field approximation in electromagnetic scattering. *Journal of Quantitative Spectroscopy and Radiative Transfer*, 100(1):268–276, 2006.

[15] Thomas Gerstner and Peter E Kloeden. *Recent developments in computational finance: foundations, algorithms and applications*, volume 14. World Scientific, 2013.

[16] Armand Wirgin. The inverse crime. *arXiv preprint math-ph/0401050*, 2004.

[17] Urs Kirchgraber, Andreas Kirsch, and Daniel Stoffer. Ill-posed problems - or, when inaccuracy is more accurate. (schlecht gestellte probleme - oder wenn das ungenaue genauer ist.). *Mathematische Semesterberichte*, 51(2):175–205, 2004. ISSN 0720-728X.

[18] Thomas S Angell and Andreas Kirsch. *Optimization methods in electromagnetic radiation*. Springer Science & Business Media, 2004.

[19] Otmar Scherzer. The use of morozov's discrepancy principle for tikhonov regularization for solving nonlinear ill-posed problems. *Computing*, 51(1):45–60, 1993.

Appendices

A The Far and Near Field of Electromagnetic Fields

The near and far field are regions of the electromagnetic field either around an object, like a transmitting antenna, or caused by radiation scattering off an object. The electromagnetic radiation in these cases has three parts: (1) the near field, (2) the transition zone and (3) the far field. Although there is no agreed location where the different regions begin and end, (different sources report different cut-off values for each,) the three distinct regions have differing properties. Qualitatively, the far-field region can be described as the region where the outgoing electric and magnetic waves are stable plane waves, or in other words, "the total scattered field is a unified outgoing spherical wave."[14] The near field, on the other hand, there is no simple representation for the electromagnetic field; the reflected and incident waves interfere to create a rather 'messy' field. In the transition region, although the field is not a unified wave as it is in the far field, there is more structure and thus it can be represented as "a superposition of outgoing spherical wavelets generated by the elementary volume elements of the object."[14] Mathematically, there are three main criteria that the far field satisfied, as is discussed in "Far-field approximation in electromagnetic scattering" by Michael I. Mishchenko. These conditions are:

$$\begin{aligned} k_1(r-a) &>> 1\,, \\ r &>> a\,, \\ r &>> \frac{k_1 a^2}{2}\,, \end{aligned}$$

where k is the wavenumber, r is the direction of propagation of the outgoing radial wave and a is the radius of the smallest circumscribing sphere of the scattering object.[14] These conditions are always satisfied in the far field; however, the near field does not satisfy any of them. For more information on the near and far field regions of electromagnetic radiation and a discussion of the above farfield conditions the reader is directed to [14].

B The Schrödinger Equation

From conservation of energy we obtain the eigenvalue problem:

$$H\Phi = E\Phi.$$

As we can see from this expression, the Hamiltonian operator H corresponds to the total energy of the system, namely the sum of potential and kinetic energy: $H = \hat{T} + \hat{V}$. From the classical counterpart, we know that the kinetic energy can be written in terms of momentum as follows:

$$T = \frac{1}{2}mv^2 = \frac{1}{2m}(mv)^2 = \frac{1}{2m}p^2\,.$$

In quantum physics, the momentum operator is given by

$$\hat{p} = -i\hbar\frac{\partial}{\partial x}\,.$$

Substituting this back into the expression for kinetic energy we obtain that

$$\hat{T} = \frac{1}{2m}\left(-i\hbar\frac{\partial}{\partial x}\right)^2 = \frac{-\hbar^2}{2m}\frac{\partial^2}{\partial x^2}\,.$$

Once again letting the Hamiltonian operator act upon the wave function Φ we get the final result:

$$E\Phi = \frac{-\hbar^2}{2m}\frac{\partial^2}{\partial x^2}\Phi + \hat{V}\Phi\,.$$

C Separation of Variables

The scalar wave equation is given by

$$\frac{\partial^2}{\partial t^2} u = c^2 \Delta u \,. \tag{23}$$

The Helmholtz equation can be derived from the scalar wave equation by separation of variables. Thus, using

$$u(x,t) = u(x)u(t)\,.$$

we obtain that,

$$\begin{aligned} \Delta u &= u''(x)u(t)\,, \\ \frac{1}{c^2}\frac{\partial^2 u}{\partial t^2} &= \frac{1}{c^2} u(x)u''(t)\,. \end{aligned}$$

Hence, the following expression is derived:

$$\begin{aligned} u''(x)u(t) &= \frac{1}{c^2} u(x)u''(t)\,, \\ \frac{u''(x)}{u(x)} &= \frac{1}{c^2}\frac{u''(t)}{u(t)}\,. \end{aligned}$$

Note that therefore $\frac{u''(x)}{u(x)}$ and $\frac{1}{c^2}\frac{u''(t)}{u(t)}$ both have to be constant. Therefore, I can write that:

$$\frac{u''(x)}{u(x)} = \frac{1}{c^2}\frac{u''(t)}{u(t)} = \mu\,,$$

where μ is an arbitrary constant. μ can be either positive, negative or zero; nevertheless, the non-trivial solution is obtained when μ is negative; hence, we define $\mu \equiv -k^2$. Therefore, defining $k \equiv {}^{\omega}/_{c_0}$, we obtain:

$$\begin{aligned} \frac{u''(x)}{u(x)} &= -k^2\,, \\ u''(x) &= -k^2 R(x)\,, \\ u(x) &= \alpha\cos(kx) + \beta\sin(kx). \end{aligned}$$

This can be checked by taking the second derivative of $u(x)$.

$$\begin{aligned} u(x) &= \alpha\cos(kx) + \beta\sin(kx)\,, \\ u'(x) &= k\beta\cos(kx) - k\alpha\sin(kx)\,, \\ u''(x) &= -k^2\alpha\cos(kx) - k^2\beta\sin(kx)\,, \\ &= -k^2(\alpha\cos(kx) + \beta\sin(kx)\,, \\ &= -k^2 u(x)\,. \end{aligned}$$

Similarly,

$$\begin{aligned} \frac{u''(t)}{u(t)} &= -c^2k^2\,, \\ u''(t) &= -c^2k^2u(t)\,, \\ u(t) &= a\cos(ckt) + b\sin(ckt)\,, \end{aligned}$$

and

$$
\begin{aligned}
u(x,t) &= u(x)u(t)\,, \\
&= (\alpha\cos(kx) + \beta\sin(kx))(a\cos(ckt) + b\sin(ckt))\,, \\
&= a\alpha\cos(kx)\cos(ckt) + b\beta\sin(kx)\sin(ckt) + a\beta\sin(kx)\cos(ckt) + b\alpha\cos(kx)\sin(ckt)\,, \\
&= A\cos(kx)\cos(ckt) + B\sin(kx)\sin(ckt) + C\sin(kx)\cos(ckt) + D\cos(kx)\sin(ckt)\,, \\
&= (A+B)\cos(kx - ckt) + (C+D)\sin(kx + ckt)\,.
\end{aligned}
$$

D A Polarized Field of Monochromatic Waves

Consider an electric field $E(x,t) = \mathscr{E}(x)T(t)$ where

$$\mathscr{E}(x) = \begin{pmatrix} \mathscr{E}_{x_1} \\ \mathscr{E}_{x_2} \\ \mathscr{E}_{x_3} \end{pmatrix} = \begin{pmatrix} \mathscr{E}_{x_1}(x_1,x_2,x_3) \\ \mathscr{E}_{x_2}(x_1,x_2,x_3) \\ \mathscr{E}_{x_3}(x_1,x_2,x_3) \end{pmatrix} .$$

Thus,

$$E(x,t) = \begin{pmatrix} \mathscr{E}_{x_1}(x_1,x_2,x_3,t) \\ \mathscr{E}_{x_2}(x_1,x_2,x_3,t) \\ \mathscr{E}_{x_3}(x_1,x_2,x_3,t) \end{pmatrix} .$$

Now suppose that the wave is polarized in the x_3 axis. This means that $\mathscr{E}_{x_1} = \mathscr{E}_{x_2} = 0$. Moreover, the resulting wave $\mathscr{E}_{x_3}$ does not depend on the third component of space, i.e.

$$E(x,t) = \begin{pmatrix} 0 \\ 0 \\ \mathscr{E}_{x_3}(x_1,x_2,t) \end{pmatrix} .$$

Hence, for a monochromatic wave polarized in the x_3 direction, the resulting field is given by:

$$E(x,t) = (0,0,\mathscr{E}_{x_3}(x_1,x_2,t))^T .$$

Maxwell's equations imply that $\mathscr{E}$ satisfies the scalar wave equation, i.e., considering a homogeneous medium, $\mathscr{E}$ is a plane wave of the form $A(x,t) = A_0\cos(k\cdot x - \omega t + \varphi)$. Nevertheless, a mathematically more versatile formulation is given using the complex number plane:

$$\begin{aligned} U(x,t) &= A_0 e^{i(k\cdot x - \omega t + \varphi)} , \\ &= A_0\cos(k\cdot x - \omega t + \varphi) + iA_0\sin(k\cdot x - \omega t + \varphi) , \\ &= A(x,t) + iA_0\sin(k\cdot x - \omega t + \varphi) , \end{aligned}$$

Thus,

$$\begin{aligned} \mathscr{E} = A(x,t) &= \mathrm{Re}(U(x,t)) = \mathrm{Re}(A_0 e^{i(k\cdot x - \omega t + \varphi)}) , \\ &= \mathrm{Re}(A_0 e^{i(k\cdot x} e^{-i\omega t} e^{i\varphi)}) , \\ &= \mathrm{Re}(u(x) e^{-i\omega t}) , \end{aligned}$$

where $u(x) \equiv e^{ik\cdot x}$, A_0 is normalized to 1 and $\varphi = 0$.

E The Sommerfeld Radiation Condition

When formulating a wave propagation problem with the Helmholtz equation, the solution isn't necessarily unique. In other words, the problem is ill-posed according to the definition posed by Hadamard. (See section 1.1 for the definition of a well-posed problem.) Take for instance the case of the scattering of sound, or the diffraction of light: The mathematical formulation of the problem has a solution that does not only provide the expected outgoing waves, i.e. the scattered waves, but also allows for incoming waves that originate at infinity and move towards the scatterer. The latter kind of waves are physically meaningless. This ill-posedness motivated theoretical physicist Arnold Johannes Wilhelm Sommerfeld to devise a criterion that singled out the meaningful outgoing waves and discarded the meaningless ones in order to provide a unique solution for the wave propagation problem. Since its introduction, this condition has become crucial for establishing the uniqueness in propagation problems and has stimulated a mathematical research.[8]
Prior to the introduction of the Sommerfeld radiation condition in 1912, uniqueness questions had been resolved by appealing to physical consideration, but, as phrased by Steven H. Schot in "Eighty years of Sommerfeld's radiation condition", "to a person with Sommerfeld's mathematical background these artifices must have seemed contrived". Thus, Sommerfeld devised a condition, applied at infinity, such that

$$\lim_{r\to\infty} r\left(\frac{\partial u}{\partial r} - iku\right) = 0 \tag{24}$$

uniformly with respect to all directions in which the limit is approached for a wave u that satisfies the Helmholtz equation. (Note that $r = \sqrt{x_1^2 + x_2^2 + x_3^2}$ in 3 dimensions.) In words, the condition singles out the outgoing wave from the incoming wave (which also satisfies the Helmholtz equation) by assuming that the propagation of the wave we're interested in to be radially outwards. Since then, this condition has taken on different forms to accommodate for a variety of different problems. According to Schot, the Sommerfeld radiation condition has "has become the standard and indispensable criterion used to ensure the uniqueness of the solution for these types of problems in mathematical physics" and "has also stimulated a considerable amount of research on uniqueness theorems for these problems from a purely mathematical standpoint."[8]

F Kirchoff Approximation

Another method used to solve the inverse Helmholtz equation is the Kirchoff approximation. This method applies to a perfectly reflecting scatterer as presented in section 2.2.1. First, take the value ka, where k is the wavenumber and a is the diameter of the 'inscribed circle to D', to be large. Moreover, take the scatterer to be smooth and convex. Under these assumptions, ${}^{\partial u}/_{\partial v}$ can be approximated by the (high-frequency) Kirchoff approximation. The Kirchoff approximation is based on the assumption that the shadow is total and that the reflection in the illuminated zone can be approximated by locally linear scatterers[1]; mathematically this means

$$\frac{\partial u}{\partial v} \simeq \begin{cases} 2\frac{\partial u^i}{\partial v}(x,d) & \text{if } x \in \partial D_d^+ \\ 0 & \text{if } x \in \partial D_d^- \end{cases}, \tag{25}$$

where $u^i(x,d) = e^{ikx\cdot d}$ Before we proceed, we first define the illuminated zone and shadow zone is defined by

$$\partial D_d^+ = \{x \in \partial D | v \cdot d < 0\}$$

and

$$\partial D_d^- = \{x \in \partial D | v \cdot d > 0\}$$

respectively, where v is the outward normal to D. Using the Kirchoff approximation we obtain the following expression for the far field pattern:

$$u_\infty(\hat{x},d) \simeq \frac{-2e^{i\pi/4}}{\sqrt{8\pi k}} \int\limits_{\partial D_d^+} \frac{\partial u^i}{\partial v}(y,d) e^{-ik\hat{x}\cdot y} ds(y)\,. \tag{26}$$

Moreover, using the far field patter we obtain that

$$e^{i\pi/4}u_\infty(\hat{x},d) + e^{-i\pi/4}u_\infty(-\hat{x},-d) \approx \frac{-2}{\sqrt{8\pi k}} \int\limits_D \frac{\partial u^i}{\partial v}(y,d) e^{-ik\hat{x}\cdot y} ds(y)\,, \tag{27}$$

$$\approx \frac{2k^{2/3}}{\sqrt{8\pi}} \int\limits_D (1 - d\cdot\hat{x}) e^{ik(d-\hat{x})\cdot y} ds(y)\,, \tag{28}$$

where expression (28) is obtained using Green's theorem and that u^i is a plane wave. In order to simplify the expression, we consider "back scattered data", which is obtained when data is only measured at the transmitter, so $d = -\hat{x}$:

$$e^{i\pi/4}u_\infty(\hat{x},d) + e^{-i\pi/4}\overline{u_\infty(-\hat{x},\hat{x})} \approx \frac{4k^{2/3}}{\sqrt{8\pi}} \int\limits_D e^{-2ik\hat{x}\cdot y} ds(y)\,, \tag{29}$$

something something fourier transform and back scattered data with certain parameters. The advantage of this method is that only back scattered data is required, rather than multistatic data that is more difficult to measure. Moreover, it makes "critical use of data for a range of wavenumbers." The main disadvantage of this method is that it only applies to convex scatterers and high-frequency data.[1]

G The Inverse Crime

To test a theoretical model, like for instance as done in the Linear Sampling Method presented in this paper, synthetic data is constructed. The creation of this data also requires a theoretical model, which, in theory, can be identical to the theoretical model employed in the first place. The term ”inverse crime” was first coined in a book by David L. Colton and Rainer Kress and refers to doing just that: use the same model to generate, as well as to invert, synthetic data. According to Colton and Kress, ”it is crucial that the synthetic data be obtained by a forward solver which has no connection to the inverse solver.”[15] In the article ”The inverse crime”, Armand Wirgin goes on to discuss: ”i) What does the term ”no connection” mean? ii) provided a definition can be given, what kind of reconstructions of the unknown parameters can one obtain when there is ”no connection” between the forward and inverse solvers? iii) should the inverse crime always be avoided? and iv) are inverse crime inversions always trivial?[16] The main issue that arises from committing the so-called inverse crime, is that the numerical algorithm may lead to unrealistically optimistic results. Regardless, according to the authors of both [15] and [17], ”inverse crimes are not possible in situations where actual real-world measured data are used, they are only a problem of computational simulation studies.”

For the case of the Linear Sampling Method, it suffices to understand that the synthetic approximation $u_\infty^{\text{comp}}(d_l, d_m)$ of $u_\infty(d_l, d_m)$ computed has to be perturbed to avoid this inverse crime, as is presented in section 4.1. By doing so, the theoretical model applied for simulating the data is no longer identical to the one used to invert the data, thereby preventing the inverse crime. For more information on the inverse crime, the reader is directed to the article [17] or any other authors cited in this section.

H Rellich's Uniqueness Lemma

Rellich's uniqueness lemma, named after austrian mathematician Franz Rellich, like Sommerfeld's radiation condition, ensures a unique solution. The lemma describes a fundamental difference between solutions of the Helmholtz equation and solutions of the Laplace equation ($\Delta u = 0$). Where some solutions of the Laplace equation can decay as ${}^{1}/_{r^m}$ for $r \to \infty$ for any $m \in \mathbb{N}$, this is not the case for solutions of the Helmholtz equation for real $k > 0$.[18]
The lemma is as follows: Assuming that u is a solution of the Helmholtz equation, in the region $\{x \in \mathbb{R}^2 : r > D\}$ for some $D > 0$, and

$$\lim_{r\to\infty} \int |u(x)|^2 dl = 0 \tag{30}$$

then u vanishes for $x > D$. In other words, Rellich's uniqueness lemma implies that the mapping of u onto its far field pattern u_∞ is one-to-one.[18] The lemma was first proven in 1943, independently by both Rellich himself and Georgian mathematician Ilia Vekua.

I Tikhonov Regularization and the Morozov Discrepancy Principle

For the Linear Sampling Method discussed in section 4, the indicator function g_z is sought for the following equation:

$$A^\delta \overrightarrow{g_z} = b_z.$$

More generally, this is a problem of the form $F(x) = y_0$ where $F : D(F) \subset X \to Y$. Since it is ill-posed, we define a solution as an "x^*-minimum-norm-solution" (MNS) x_0, as presented by Otmar Scherzer in "The Use of Morozov's Discrepancy Principle for Solving Nonlinear Ill-Posed Problems". In mathematical terms, this means that we define an x_0 such that

$$F(x_0) = y_0$$

and

$$||x_0 - x^*|| = \min_{x \in D(F)} \{||x - x^*|| : F(x) = y_0\}.$$

It is assumed that there exists such a solution for the exact data y, although due to the nonlinearity of F the solution is not necessarily unique. In fact, as is the case with the Helmholtz equation, when $F(x) = y_0$ is ill-posed due to a lack of continuity of its solutions with respect to the data (criterion 3 of Hadamard's definition of a well-posed problem, introduced in section 1.1) regularization techniques are required. The regularization technique employed by Cakoni et. al. in [1] is called Tikhonov regularization and works as follows: an approximation of the solution is obtained through the minimization problem defined by

$$\min_{x \in D(F)} \left\{ ||F(x) - y^\delta||^2 + \alpha ||x - x^*||^2 \right\},$$

where the α is the regularization parameter ($\alpha > 0$) and $y^\delta \in Y$ is the "available noisy data" for which it holds that $||y^\delta - y_0|| \leq \delta$.[19] Note that for the LSM, in section 4.1 A^δ is used to denote the available data instead of y^δ and $||A - A^\delta|| \leq \delta$ is assumed. Moreover, ror the LSM this translates to the equation (18) given in section 4.1.

In order to proceed with Tikhonov regularization, a regularization parameter α has to be chosen accordingly; a priori methods exist where the choice of α depends on the level of noise δ and certain smoothness assumptions, which are in practice extremely difficult to verify. This is an issue because a poor choice of α leads to a bad approzimation of the MNS. The best choice for the regularization parameter α is "as large as possible"; smaller regularization parameters mean more numerical instabilities.[19] According to Scherzer, a priori methods can lead to the choice of α to be too small. A posteriori strategies, on the other hand, establish a regularization parameter from "quantities that arise during calculations" without using the unreliable smoothness assumptions that a priori methods rely on. The, according to Scherzer, "most famous discrepancy principle" is the one used by Cakoni et. al. for the LSM: Morozov's discrepancy principle.

I.1 Morozov's Discrepancy Principle

Morozov's discrepancy principle chooses the regularization parameter α for the Tikhonov regularization as presented above, such that

$$||F(x_\alpha^\delta) - y_\delta||^2 = c\delta^2,$$

where $c > 1$. This can be rewritten in terms of the inverse problem to which the LSM is applied in section 4.1 to get:

$$||A^\delta \overrightarrow{g}_z^\alpha - b_z||^2 = \delta^2 ||\overrightarrow{g}_z^\alpha||^2. \tag{31}$$

Following the reasoning presented by Cakoni et. al., this can be computed using "singular value decomposition" of A^δ, i.e.

$$A^\delta = USV^*.$$

U and V are, like A^δ, $N \times N$ matrices, both unitary. S is a diagonal matrix with $S_{i,i} = \sigma_i \geq 0$. Since U is unitary, we obtain that

$$||A^\delta \overrightarrow{g}_z^\alpha - \overrightarrow{b}_z|| = ||SV^* \overrightarrow{g}_z^\alpha - U^* \overrightarrow{b}_z|| \,.$$

For the right hand side of equation (31), we use the fact that V is unitary such that

$$||\overrightarrow{g}_z^\alpha|| = ||V^* \overrightarrow{g}_z^\alpha|| \,.$$

Moreover, the Tikhonov regularization problem discussed in section 4.1 can be rewritten as follows:

$$\begin{aligned} \left(\alpha_z I + \left(A^\delta\right)^* A^\delta\right) \overrightarrow{g}_z^\alpha &= \left(A^\delta\right)^* \overrightarrow{b_z} \,, \\ \left(\alpha_z I + VS^2V^*\right) \overrightarrow{g}_z^\alpha &= VSU^* \overrightarrow{b_z} \,, \\ \left(\alpha_z I + S^2\right) \left(V^* \overrightarrow{g}_z^\alpha\right) &= SU^* \overrightarrow{b_z} \,. \end{aligned}$$

Next, Cakoni et. al. define $\overrightarrow{v}^\alpha = V^* \overrightarrow{g}_z^\alpha$ to obtain the expression

$$\overrightarrow{v}^\alpha = (\alpha_z + \sigma_i^2)^{-1} \sigma_i (U^* \overrightarrow{b}_z)_i, \qquad\qquad i = 1, ..., N \,.$$

Hence,

$$||A^\delta \overrightarrow{g}_z^\alpha - b_z|| = \sum_{i=1}^N \left(\frac{\alpha_z}{\alpha_z + \sigma_i^2}\right)^2 |(U^* b_z)_i|^2 \,,$$

$$||\overrightarrow{g_z}||^2 = \sum_{i=1}^N \left(\frac{\sigma_i}{\alpha_z + \sigma_i^2}\right)^2 |(U^* b_z)_i|^2 \,.$$

Thus α is the zero of

$$f(\alpha) = \sum_{i=1}^N \frac{\alpha^2 - \delta^2 \sigma_i^2}{(\sigma_i^2 + \alpha)^2} |(U^* b_z)_i|^2 \,. \tag{32}$$

J Full Python Programme

```
import numpy as np
import scipy as sp
from matplotlib import pyplot as plt


file=open("C://Users//Jocelijn//Desktop//Thesis//Python//datafile.exp.txt")

#FILTERING FOR A SINGLE FREQUENCY
frequency_GHz=int(input("frequency requested: "))

filtered=[]#will contain data filtered for requested frequency
for line in file:
   line = line.strip()
   data=line.split()
   if data[0]!='#':#ignore lines of text that isn't data
       frequency=int(data[2])
       if frequency == frequency_GHz:
           filtered.append(data)

L=[]#will contain matrix argument
n=1#index for angle of emission
while n<=36:
    a=0#index for angle of reception
    wavefield=[0]*(12+n-1)#accounting for missing measurements
    while a<len(filtered):
        if filtered[a][0]==str(n):
            real_part=float(filtered[a][3])-float(filtered[a][5])
            complex_part=float(filtered[a][4])-float(filtered[a][6])
            wavefield.append(complex(real_part,complex_part))#scattered wave
        a+=1
    wavefield.extend(0 for i in range(12+36-n))#accounting for missing measurements
    L.append(wavefield)
    n+=1
data_matrix=np.matrix(L)

#PLOTTING THE REAL PART OF THE DATA MATRIX
plt.matshow(np.real(data_matrix))
plt.show()

#SOLVING FOR g
def computation(z,alpha):#computes the norm of the indicator function for one coordinate z
    #needed constants:
    radius=0.76
    c=sp.constants.c#speed of light
    frequency_Hz=int(frequency_GHz)*10**9
    omega=frequency_Hz*2*np.pi#angular frequency
    k=omega/c#wavenumber
```

```
    N=int(data_matrix.shape[0])
    h=(2*np.pi)/N
    frac=np.e**(1j*np.pi/4)
    sq=np.sqrt(8*np.pi*k)


    list1=[x for x in range(data_matrix.shape[0])]#angle index
    phi=[]
    Phi=[]
    for angle in list1:
        x=np.asarray((radius*np.cos(np.radians(angle*10)),radius*np.sin(np.radians(angle*10))))
        Phi.append((frac/sq)*np.e**(-1j*k*np.dot((x/np.linalg.norm(x)),z)))#phi_infty
        phi.append((1j/4)*sp.special.hankel1(0,k*np.linalg.norm(x-z)))#phi
    n=0
    while n<len(phi):
        phi[n] = (1/h)*phi[n]
        Phi[n] = (1/h)*Phi[n]
        n+=1

    b1=np.array(Phi)#vector b
    b2=np.array(phi)#alternative vector b

    transpose=data_matrix.getH()
    U=np.dot(transpose,data_matrix)

    identity=np.identity(U.shape[0])
    A=(alpha*identity)+U

    B1=np.dot(transpose,b1)
    B2=np.dot(transpose,b2)

    g1=np.linalg.solve(A,B1.transpose())
    g2=np.linalg.solve(A,B2.transpose())

    return np.linalg.norm(g1)#gives norm of indicator function

n=0.2
z=np.asarray((-n,-n))#first coordinate z
alpha=raw_input("regularization constant requested: ")#regularization constant
if alpha == "":
    alpha=1e-6

W=[]
#choosing multiple z
while z[1] <= n:
    L=[]
    while z[0] <= n:
        #print(z)
        L.append(computation(z,alpha))
```

```
        z[0]+=0.01
    z[1]+=0.01
    z[0]=-n
    W.append(L)

#FINAL RESULT
result=np.matrix(np.asarray(W))
plt.matshow(np.real(result))
plt.show()
```

K Programme Results for Data by Belkebir and Saillard

K.1 Single Dielectric

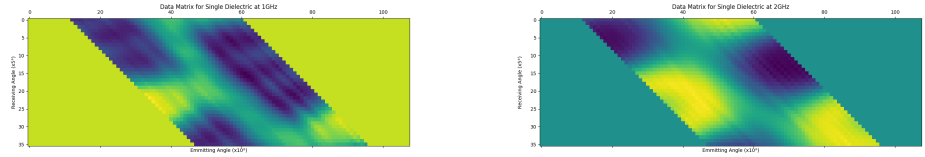

(a) frequency = 1 GHz (b) frequency = 2 GHz

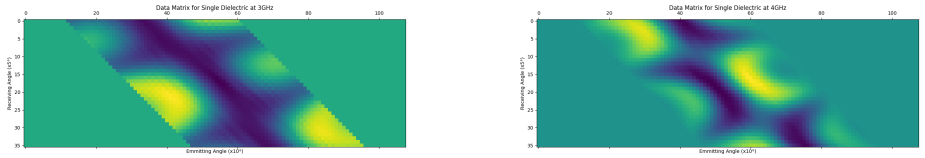

(c) frequency = 3 GHz (d) frequency = 4 GHz

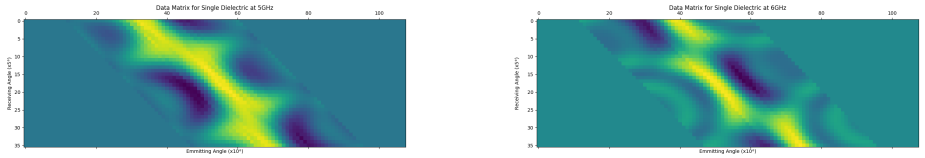

(e) frequency = 5 GHz (f) frequency = 6 GHz

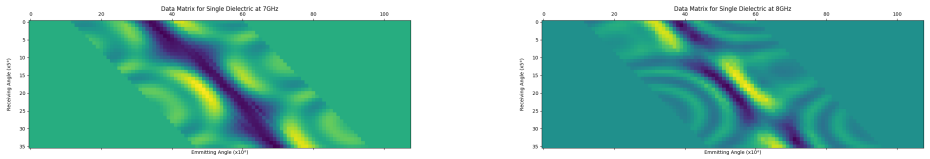

(g) frequency = 7 GHz. (h) frequency = 8 GHz.

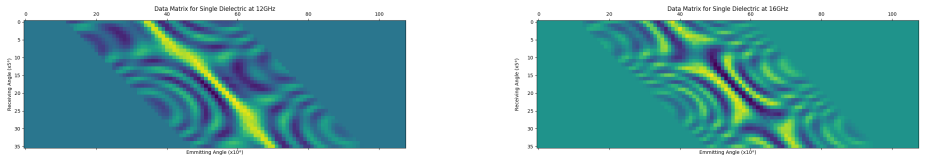

(i) frequency = 12 GHz. (j) frequency = 16 GHz.

Figure 10: Data matrices of a single dielectric for a range of frequencies obtained from the data in [11].

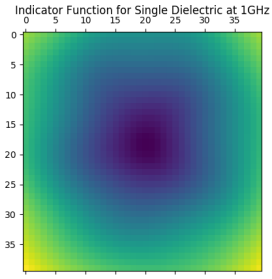

(a) frequency = 1 GHz.

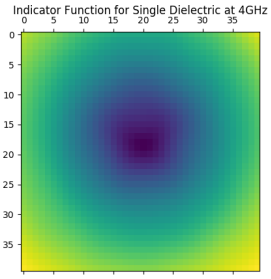

(b) frequency = 2 GHz.

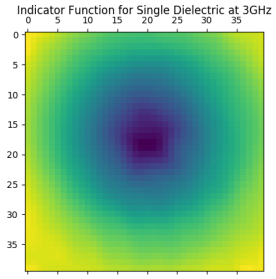

(c) frequency = 3 GHz.

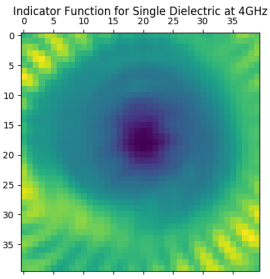

(d) frequency = 4 GHz.

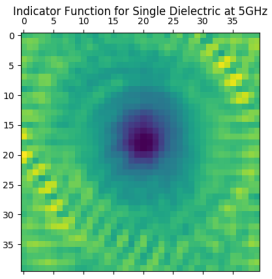

(e) frequency = 5 GHz.

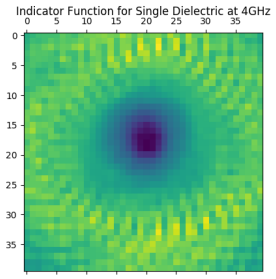

(f) frequency = 6 GHz.

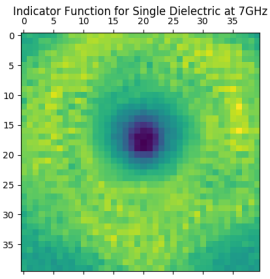

(g) frequency = 7 GHz.

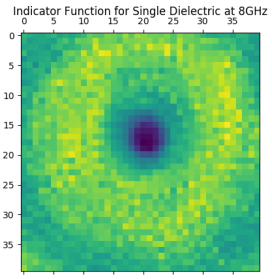

(h) frequency = 8 GHz.

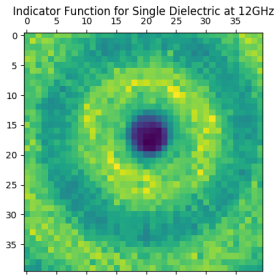

(i) frequency = 12 GHz.

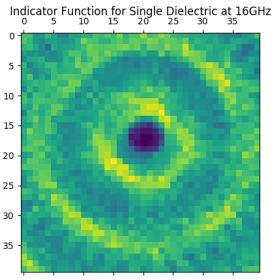

(j) frequency = 16 GHz.

Figure 11: Indicator function of a single dielectric for a range of frequencies obtained from the data in [11].

K.2 Two Dielectrics

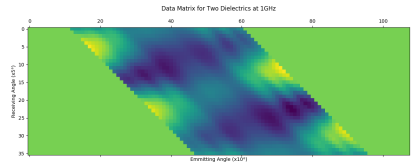

(a) frequency = 1 GHz.

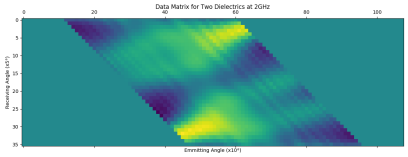

(b) frequency = 2 GHz.

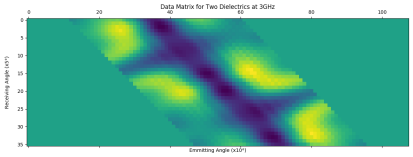

(c) frequency = 3 GHz.

(d) frequency = 4 GHz.

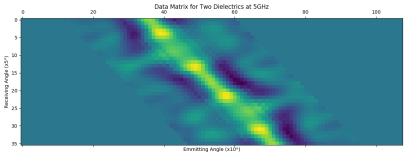

(e) frequency = 5 GHz.

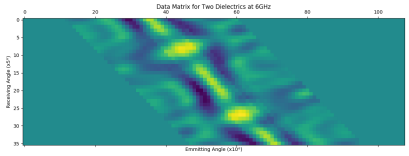

(f) frequency = 6 GHz.

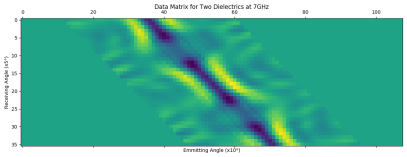

(g) frequency = 7 GHz.

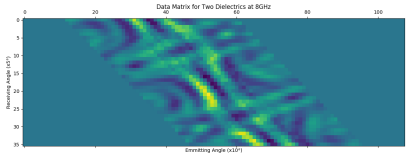

(h) frequency = 8 GHz.

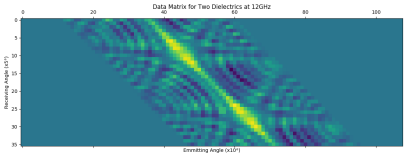

(i) frequency = 12 GHz.

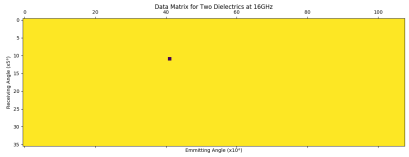

(j) frequency = 16 GHz.

Figure 12: Data matrices of two dielectrics for a range of frequencies obtained from the data in [11].

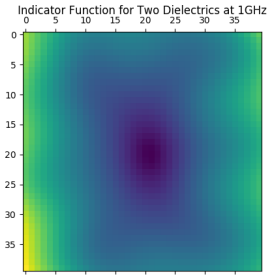

(a) frequency = 1 GHz.

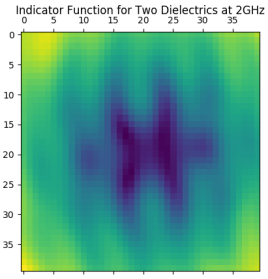

(b) frequency = 2 GHz.

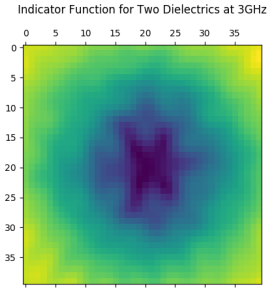

(c) frequency = 3 GHz.

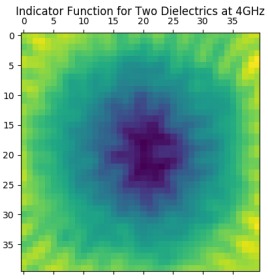

(d) frequency = 4 GHz.

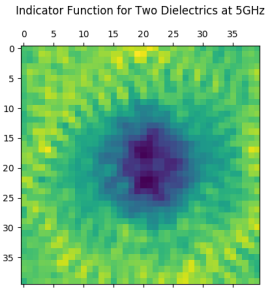

(e) frequency = 5 GHz.

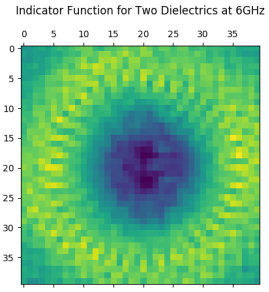

(f) frequency = 6 GHz.

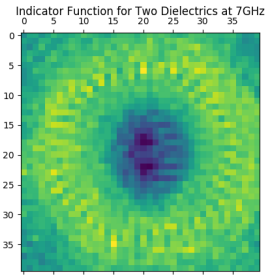

(g) frequency = 7 GHz.

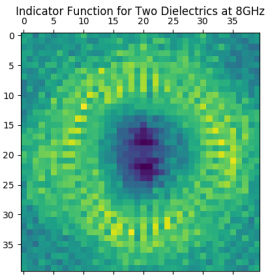

(h) frequency = 8 GHz.

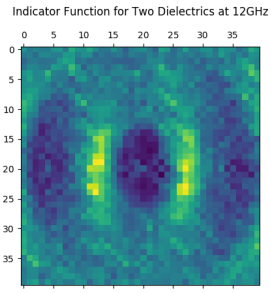

(i) frequency = 12 GHz.

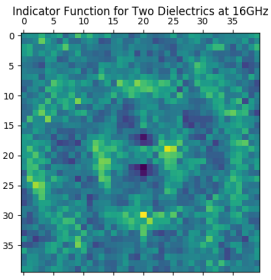

(j) frequency = 16 GHz.

Figure 13: Indicator function of two dielectrics for a range of frequencies obtained from the data in [11].

K.3 Metallic Rectangle

K.3.1 Centred

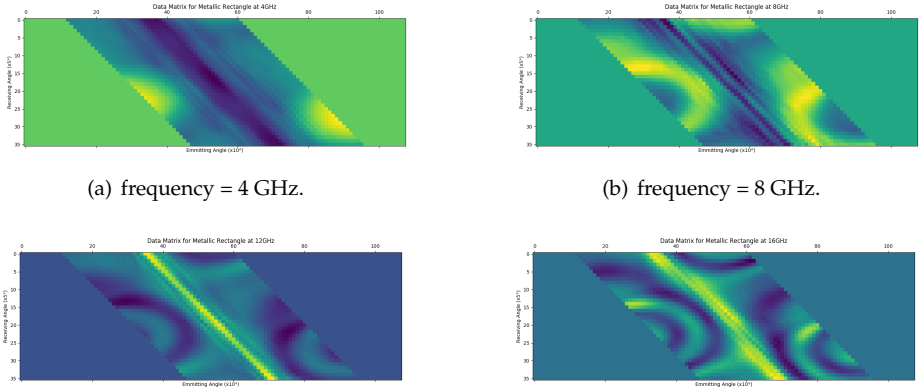

(a) frequency = 4 GHz.

(b) frequency = 8 GHz.

(c) frequency = 12 GHz.

(d) frequency = 16 GHz.

Figure 14: Data matrices of a centered metallic rectangle for a range of frequencies obtained from the data in [11].

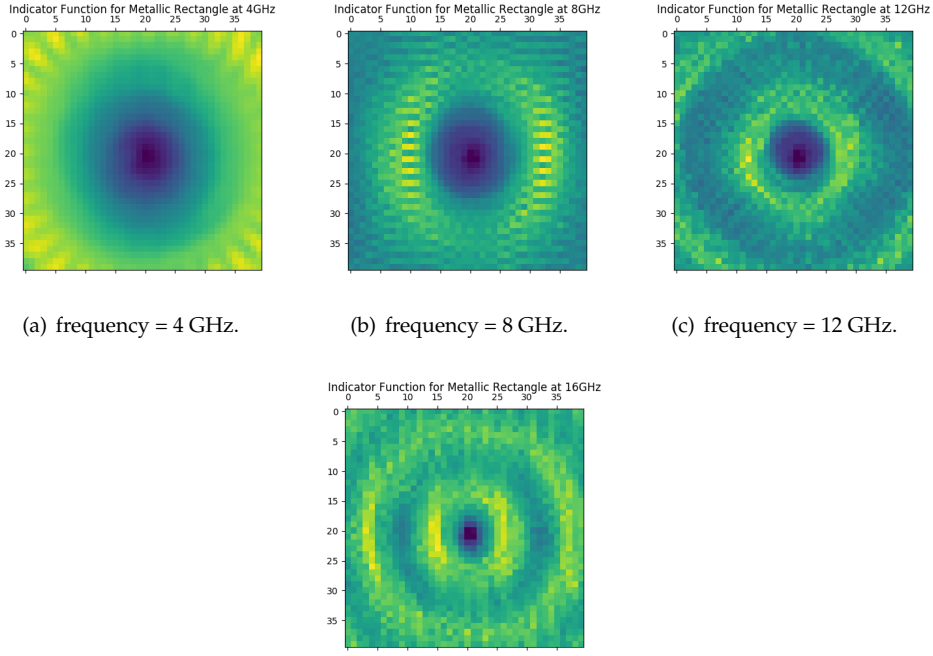

(a) frequency = 4 GHz.

(b) frequency = 8 GHz.

(c) frequency = 12 GHz.

(d) frequency = 16 GHz.

Figure 15: Indicator function of a centered metallic rectangle for a range of frequencies obtained from the data in [11].

K.3.2 Decentred

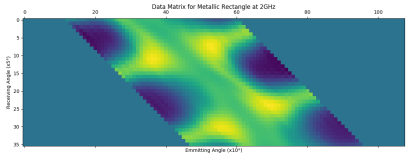

(a) frequency = 2 GHz.

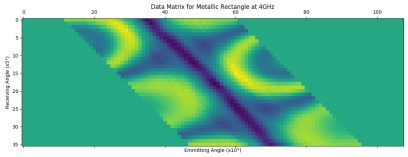

(b) frequency = 4 GHz.

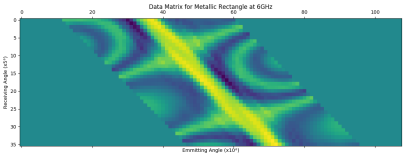

(c) frequency = 6 GHz.

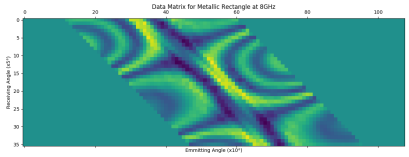

(d) frequency = 8 GHz.

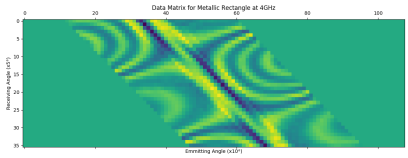

(e) frequency = 10 GHz.

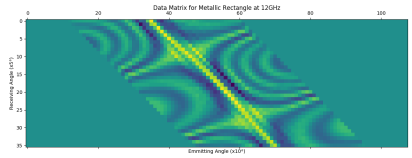

(f) frequency = 12 GHz.

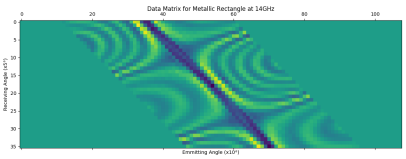

(g) frequency = 14 GHz.

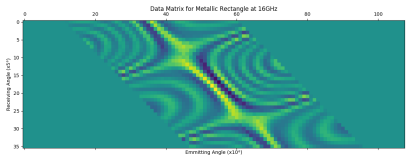

(h) frequency = 16 GHz.

Figure 16: Data matrices of a centered metallic rectangle for a range of frequencies obtained from the data in [11].

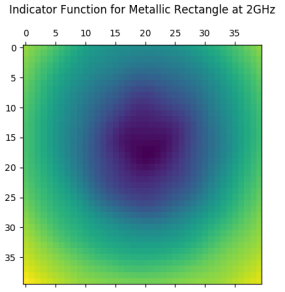

(a) frequency = 2 GHz.

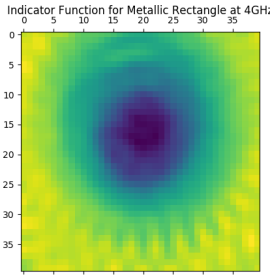

(b) frequency = 4 GHz.

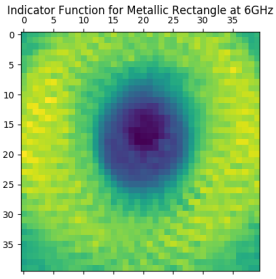

(c) frequency = 6 GHz.

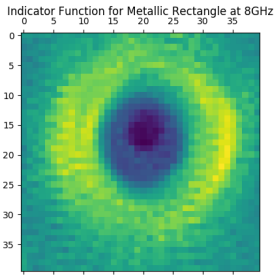

(d) frequency = 8 GHz.

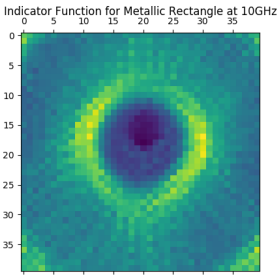

(e) frequency = 10 GHz.

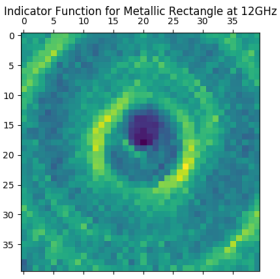

(f) frequency = 12 GHz.

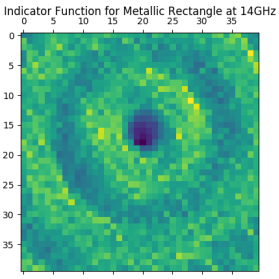

(g) frequency = 14 GHz.

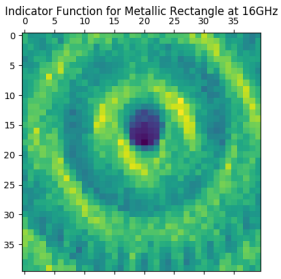

(h) frequency = 16 GHz.

Figure 17: Indicator function of a centered metallic rectangle for a range of frequencies obtained from the data in [11].

K.4 Metallic 'U'-Shape

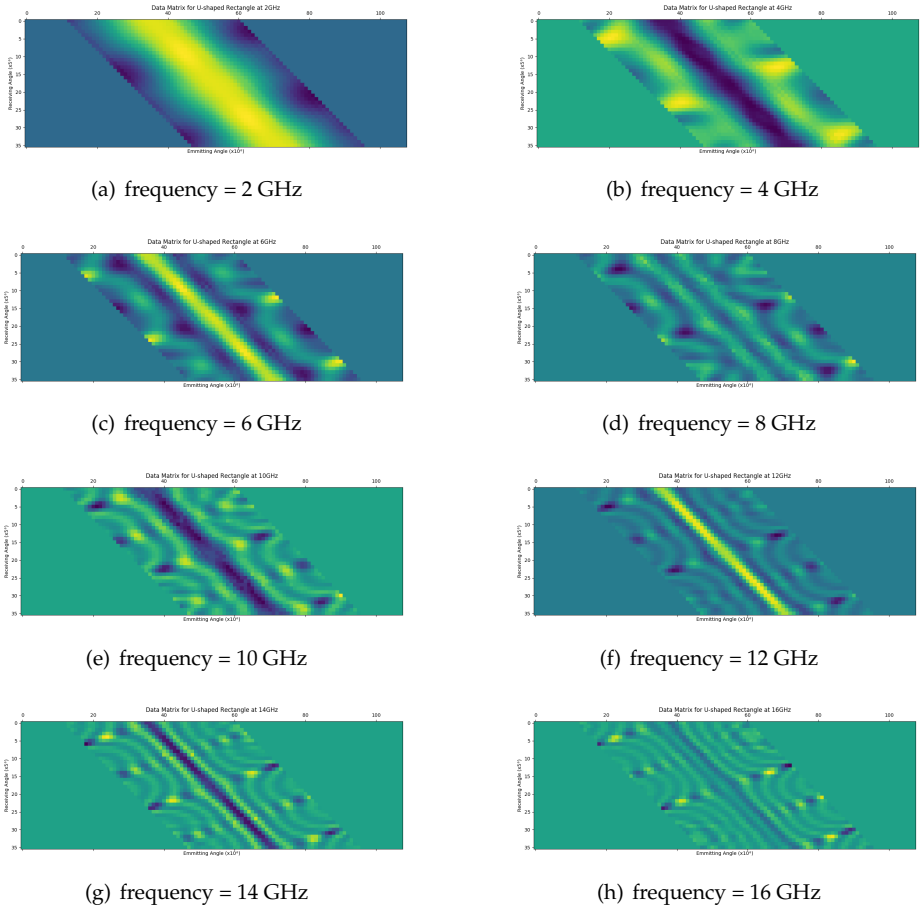

(a) frequency = 2 GHz

(b) frequency = 4 GHz

(c) frequency = 6 GHz

(d) frequency = 8 GHz

(e) frequency = 10 GHz

(f) frequency = 12 GHz

(g) frequency = 14 GHz

(h) frequency = 16 GHz

Figure 18: Data matrices of a metallic 'U'-shaped scatterer for a range of frequencies obtained from the data in [11].

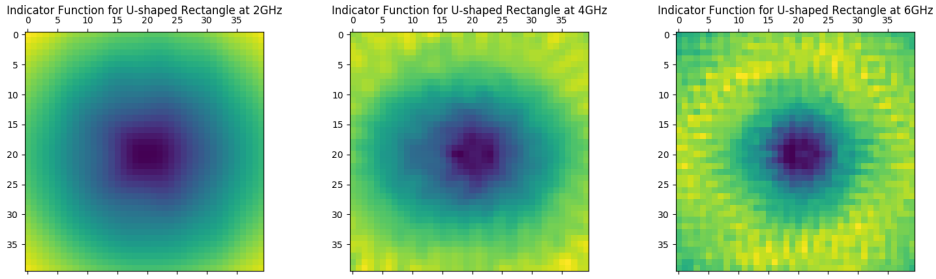

(a) frequency = 2 GHz (b) frequency = 4 GHz (c) frequency = 6 GHz

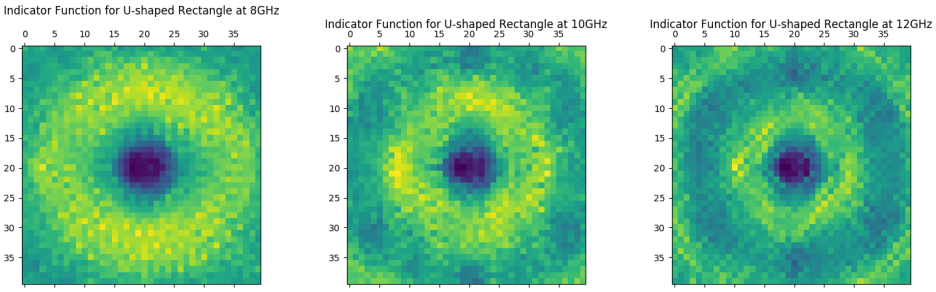

(d) frequency = 8 GHz (e) frequency = 10 GHz (f) frequency = 12 GHz

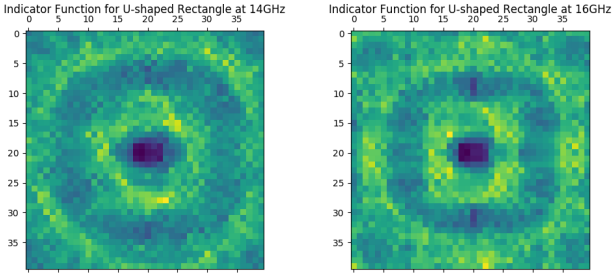

(g) frequency = 14 GHz (h) frequency = 16 GHz

Figure 19: Indicator function of a metallic 'U'-shaped scatterer for a range of frequencies obtained from the data in [11].

K.5 Effect of Regularization Parameter α

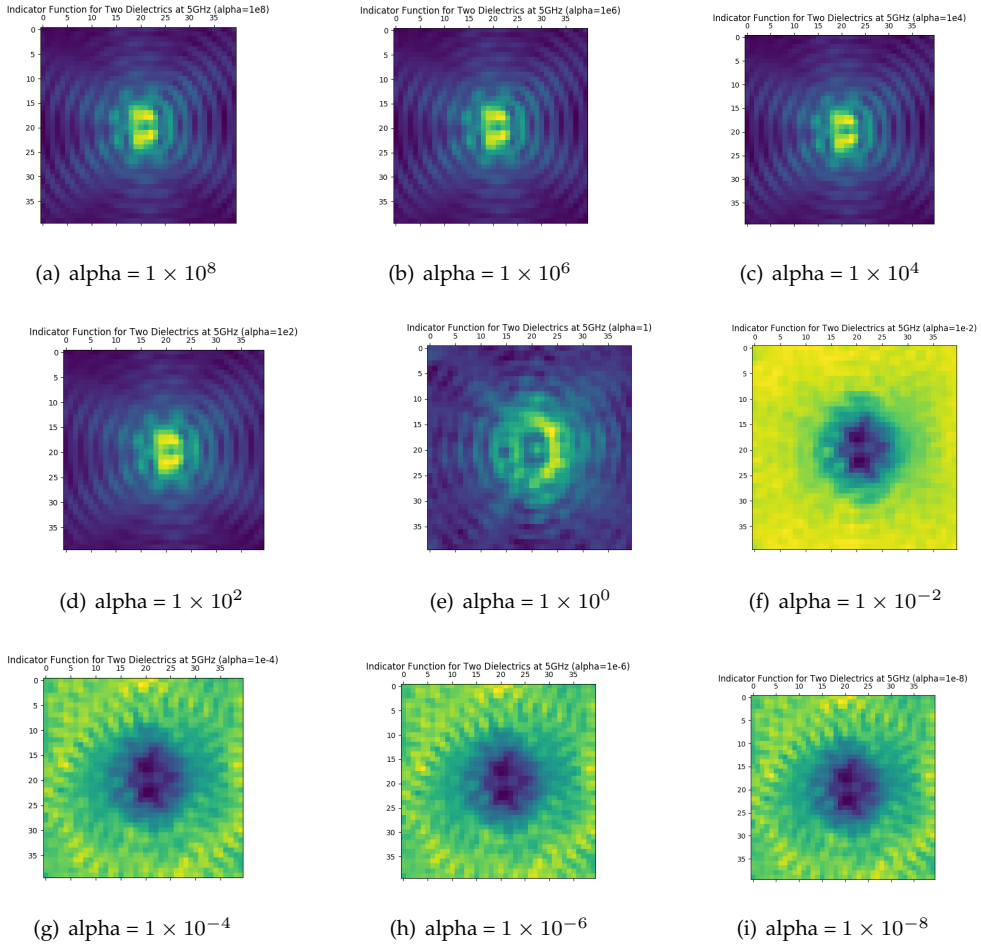

(a) alpha = 1×10^{8} (b) alpha = 1×10^{6} (c) alpha = 1×10^{4}

(d) alpha = 1×10^{2} (e) alpha = 1×10^{0} (f) alpha = 1×10^{-2}

(g) alpha = 1×10^{-4} (h) alpha = 1×10^{-6} (i) alpha = 1×10^{-8}

Figure 20: Indicator function of two dielectrics at frequency 5GHz for a range of regularization parameters α obtained from the data in [11].